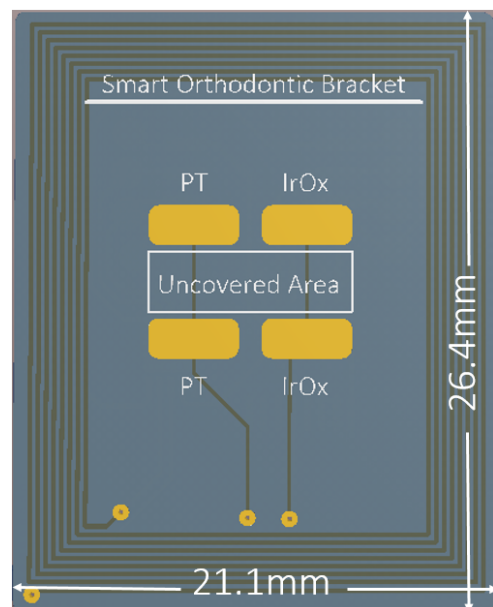


Imperial College London

Department of Electrical and Electronic Engineering

Final Year Project Report 2017



Project Title: **Smart Orthodontic Bracket for in-mouth metabolite measurements**

Student: **Daryl Ma**

CID: **00754071**

Course: **4T**

Project Supervisor: **Dr Sara S. Ghoreishizadeh**

Second Marker: **Professor Christofer Toumazou**

Abstract

An indication of the dental health of patients can be observed from the pH levels of their saliva. Thus, this project involves **the design and implementation of a wireless pH sensor for use as a Smart Orthodontic Bracket (SOB)**. This device aims to measure a pH value between 5 to 8 while being powered wirelessly. This is done whenever it is required by the user. At the same time, this pH value will be communicated wirelessly to the user. Lastly, the device has to be small enough for retrofitting in a user's mouth.

Research was carried out on three main topics: **pH sensing, energy harvesting and wireless communications**. Comparison of different pH sensing options showed that Iridium Oxide(IrOx) electrodes in tandem with a reference electrode was the most suitable due to their biocompatibility as well as their small sizes(<1cm). A read out circuit was designed for the electrodes, from which the LMP91200 integrated chip(IC) from Texas Instruments was used.

Physical energy harvesting and radio frequency energy harvesting methods were compared, from which inductive coupling arose as the likeliest energy harvesting solution due to its higher power yields(>1mW). A further review into inductive coupling was then done to determine the optimum frequency for power transmission, before the AMS AS3955 IC was chosen based on available commercial options for a 13.56MHz-based power transfer.

The wireless communications protocol used is near field communications(NFC). In order to apply this protocol, antenna design techniques as well as a comparison of available commercial antennas were tested. Lastly, the ATTiny range of low-powered microcontrollers were compared for use with the NFC protocols as well as the read out circuit. The microcontroller was run at low frequencies(125kHz) in order to ensure that minimal power was used.

Each of the modules were tested successfully before integration into a breadboard for further tests. Two printed circuit boards(PCBs) were manufactured, with the first being an experimental PCB with multiple antennas for testing, and the second being the final prototype. The final prototype collaborated with the above stated specifications.

Acknowledgements

This project has been a long and rewarding ride. It would be remiss to call it a cruise, and more appropriate to relate as an escapade into the unknown. As any adventures go, help and aid from key personnel was vital in finishing the journey.

The idea for this project stemmed from **Dr Sara S. Ghoreishizadeh**, who also supervised the entirety of the project. A big thanks for your patience and time for answering my questions, as well as encouragement through difficult periods in the research. Most importantly, for making this project enjoyable as well.

Professor Alyssa Apsel, for her help in NFC technologies and experience dealing with the prototyping of NFC antennas,

Professor Christos Papavasiliou and **Dr Steve Wright**, for guiding my initial venture into RF systems,

Dr Christine Mason, for her kind advice and time during the weekend to impart her experience as a dentist and the background medical knowledge,

Mr Vic Boddy, **Mrs May Tang** and **Mr Amin Halimi**, for their help in the 1st floor labs trying to figure out what went wrong with the circuit,

To **Mr Wei Cong Te**, for accompanying me throughout the project, and struggling together trying to find solutions, together with **Mr Drinu** from the CBIT labs,

Dr Alwyn Elliot, for bringing me around the entire EEE finding any academic who had any experience with NFC systems,

My family for allowing me to work during the weekends and giving me the opportunity to complete this degree.

Last but not least, to those in the labs who've helped me in one way or another.

Thank you for this.

Contents

Abstract	i
Acknowledgements	ii
List of Figures	vi
List of Tables	viii
Abbreviations	ix
1 Introduction	1
1.1 Project Overview	1
1.2 Device Brief	1
1.3 Report Structure	2
2 Project Background	4
2.1 Medical Background	4
2.1.1 Form Factor	4
2.1.2 Range of pH values and Frequency of Readings	5
2.2 Prior Research	5
2.3 Detailed Specifications	7
2.4 High Level Design	7
3 pH Sensing	9
3.1 Theory	9
3.2 Requirements for Module	10
3.3 Analysis of Options	10
3.3.1 Glass Electrodes	10
3.3.2 Ion-Sensitive Field Effect Transistors(ISFETS)	11
3.3.3 Iridium Oxide(IrOx) Electrodes	12
3.3.4 Fibre-Optics	13
3.4 Choice of Method	13
3.5 Readout Circuit	14
3.6 Chapter Summary	15
4 Energy Harvesting	16
4.1 Physical Energy Harvesting	16

4.1.1	Thermoelectric Harvesting	17
4.1.2	Motion Harvesting	17
4.2	RF Energy Harvesting	18
4.2.1	Infrared Radiation	18
4.2.2	Electromagnetic Inductive Coupling	18
4.3	Analysis of Options	19
4.4	Inductive Coupling	19
4.4.1	Antenna Sizes and Energy Transmitted	20
4.4.2	Penetration Depth	20
4.4.3	Alternative Viewpoints	21
4.4.4	Industrial, Scientific and Medical(ISM) Radio Bands	21
4.5	Choice of Frequency	22
4.6	Options for RF Energy Harvesting ICs	22
4.7	Chapter Summary	23
5	Wireless Communication Module	24
5.1	Near Field Communication(NFC)	24
5.1.1	NFC Methodology	25
5.1.1.1	Modulation Schemes	26
5.1.1.2	NFC Forum Type 2 Tag Platform	26
5.1.2	Comparison with other existing protocols	27
5.2	Antenna	28
5.2.1	AS3955 Required Antenna Inductance	29
5.2.2	Obtaining the antenna	29
5.2.2.1	Commercially Available Antennas	30
5.2.2.2	Designing the Antenna	31
5.3	Microcontroller	33
5.3.1	Requirements	33
5.3.2	Analysis of Options	33
5.4	Chapter Summary and Final Proposed Circuit	34
6	Individual Module Tests	36
6.1	pH Tests	36
6.1.1	Experimental Setup	36
6.1.2	Experiment 1: Linearity of Electrodes	38
6.1.3	Experiment 2: Response Time	39
6.1.4	Experiment 3: Power Consumption of the LMP91200	39
6.2	Microcontroller Tests	39
6.2.1	Experimental Setup	40
6.2.2	Experiment 1: ATTiny85 Clock Speed	40
6.2.3	Experiment 2: Analog to Digital Converters(ADCs)	43
6.2.3.1	Single and Differential Inputs	44
6.2.3.2	ADC Clock Prescaler	45
6.2.3.3	ADC Voltage Reference	45
6.2.4	Experiment 3: Universal Serial Interface(USI)	45
6.2.5	Experiment 4: Power Consumption of the ATTiny85	46
6.3	NFC Tests	46

6.3.1	Experimental Setup	46
6.3.2	Experiment 1: NFC Communication with the smartphone from the AS3955	47
6.3.3	Experiment 2: AS3955 Reader Orientation and Distances	48
6.3.4	Experiment 3: Varying the output power supply from the AS3955	49
6.3.5	Experiment 4: Varying the Antennas used on the AS3955	49
6.3.6	Experiment 5: Output Power supplied by the AS3955	50
6.4	Chapter Summary	51
7	Overall Module Tests	52
7.1	Breadboard Tests	52
7.1.1	Experimental Setup	52
7.1.2	Experiment 1: Electrodes to LMP91200	53
7.1.3	Experiment 2: LMP91200 to ATTiny85	54
7.1.3.1	ADC Accuracy	54
7.1.3.2	ADC Decoder	54
7.1.4	Experiment 3: ATTiny85 to AS3955	54
7.1.5	Experiment 4: Full System Characterisation	55
7.2	Experimental PCB	56
7.2.1	Design of Experimental PCB	56
7.2.1.1	Requirements	56
7.2.2	PCB Design	56
7.2.2.1	Electrode Pad Points	56
7.2.2.2	Testpoints and Headers	57
7.2.2.3	Antennas	57
7.2.2.4	PCB Substrate	58
7.2.3	Experiment 1: Testing NFC Antennas	59
7.2.4	Experiment 2: Ground Plane on Antenna	61
7.2.5	Experiment 3: Throughput Tests	61
7.3	Chapter Summary	63
8	Final Prototype and Evaluation	64
8.1	Final Prototyped Device	64
8.1.1	PCB Design	65
8.1.2	Encapsulation of device	66
8.2	Final Prototype Details	66
8.3	Chapter Summary and Evaluation	67
9	Conclusion and Future Work	69
9.1	Future Work	70
A	Appendix A: Embedded Software	72
	Bibliography	82

List of Figures

2.1	Proposed device fitting on different types of dental equipment	4
2.2	Block Diagram of IrOx electrode implemented circuit. Taken from [1] . .	6
2.3	IrOx Electrode Sensing Circuit. Taken from [1].	6
2.4	Overall Envisioned System of Smart Orthodontic Bracket (SOB) with required modules	8
3.1	pH sensor module with required inputs and outputs	9
3.2	Glass Electrode Configuration. Taken from [2]	11
3.3	ISFET Diagram	11
3.4	Different Electrodes used for pH sensing	12
3.5	Iridium Oxide Electrodes with Read Out Circuit	14
3.6	Iridium Oxide Electrode Proposed Read-Out Circuit	14
3.7	LMP91200 pH Sensing IC	15
4.1	Energy Harvesting Module	16
4.2	Illustration of Thermoelectric Harvesting from a user's body. Taken from [3]	17
4.3	IR Harvester Circuit Implementation. Taken from [4]	18
4.4	Inductive Coupling with Power and Data Transmission. Taken from [5] .	18
4.5	AS3955 Block Diagram. Taken from [6].	23
5.1	Wireless Communications Module	24
5.2	Near Field Communication Protocol	24
5.3	Reader and Tag System Diagram. Taken from [6].	25
5.4	Analog Front End of AS3955 Chip. Taken from [6].	26
5.5	NDEF Message Block	27
5.6	AS3955 with associated modules	27
5.7	Equivalent Circuit Model of an NFC tag in the presence of a field. Taken from [7].	28
5.8	Capacitive Compensation for NFC antennas	30
5.9	Rectangular Loop Coil. Taken from [7].	31
5.10	Panasonic NFC Antenna Online Tool. Taken from [8].	32
5.11	PCB Designed Antennas.	32
5.12	Microcontroller Module Requirements	33
5.13	Block Diagram of Proposed pH-monitoring system	34
6.1	Circuit Setup for pH Tests	37
6.2	LMP91200 Configuration	37

6.3	pH measurements acquired with fabricated IrOx electrode and three different reference electrodes: IrOx and AgCl on the top, IrOx and Ir Wire in the middle, IrOx and Pt Wire on the bottom. Linearity is stated in each figure.	38
6.4	ATTiny 85 Pinout. Taken from [9].	39
6.5	Microcontroller Tests setup	41
6.6	Clock Distribution Diagram of the ATTiny85. Taken from [9].	42
6.7	Close Source Selection. Taken from [9].	42
6.8	Clock Prescaler Select. Taken from [9].	43
6.9	ATTiny 85 ADCs Configuration. Taken from [9].	44
6.10	AS3955 Evaluation Board with NFC Tags	47
6.11	Android Software Configuration	47
6.12	Tag Operation Distance	48
6.13	Connecting the Tag to the Evaluation board	49
6.14	External Antenna for NFC Tag	50
7.1	SOB Schematic	53
7.2	Breadboard Testing	53
7.3	Flow diagram of software	55
7.4	PCB Schematic	57
7.5	PCB Layout	57
7.6	PCB 3D View	58
7.7	Fabricated PCB with components annotated.	58
7.8	Antenna Tests	59
7.9	Antenna Power Supply Tests	60
7.10	PCB Ground Plane Tests	61
7.11	Throughput Tests with Experimental PCB	62
8.1	Envisioned SOB Fitting on retainers, with SOB covered with epoxy. The SOB is placed on the outer layer of the retainers to avoid interference with user's jaw motion.	64
8.2	Final Prototype PCB Design	65
8.3	Final Prototype Schematic	65
8.4	Encapsulation Solution Set up	66

List of Tables

1.1	Project Deliverables	2
2.1	Detailed Specifications for SOB	7
3.1	pH Sensing Options	13
4.1	Evaluation of Energy Harvesting Methods	19
4.2	Energy Harvesting IC Options	22
5.1	Commercial NFC Antenna Options	30
5.2	ATTiny Microcontroller Options	34
6.1	Threshold Distance of Operation for AS3955 Tags	48
6.2	Output Voltage across Varying Load Values at a constant distance of 10mm	50
7.1	Antenna Characterization results	59
7.2	pH tests with implemented PCB	62
8.1	Summary of Components	67
8.2	Detailed Specifications for SOB	67
8.3	Comparison with state-of-the-art	68

Abbreviations

AC	Alternating Current
ADC	Analog to Digital Converter
AFE	Analog Front End
AgCl	Silver Chloride
ASK	Amplitude Shift Keying
BLE	Bluetooth Low Energy
CBIT	Centre for Bio-Inspired Technology
CS	Chip Select
DC	Direct Current
DIP	Dual-Inline Package
EEPROM	Electrically Erasable Programmable Read-Only Memory
EM	Electro Magnetic
HFSS	High Frequency Structural Simulator
IC	Integrated Circuit
I2C	Inter-Integrated Circuit
Ir	Iridium
IR	Infrared Radiation
IrOx	Iridium Oxide
ISFET	Ion Sensitive Field Effect Transistor
ISM	Industrial, Scientific and Medical
ISO	International Organisation of Standards
LC	Inductor-Capacitor
MISO	Master In Slave Out
MOSFET	Metal - Oxide -Semiconductor Field Effect Transistor
MOSI	Master Out Slave In

NDEF	NFC Data Exchange Format
NFC	Near Field Communications
PCB	Printed Circuit Board
Pt	Platinum
RF	Radio Frequency
RLC	Resistor - Inductor - Capacitor
<i>SiO₂</i>	Silicon Dioxide
SOB	Smart Orthodontic Bracket
SOIC	Small-Outline Integrated Package
SPI	Serial Parallel Interface
USB	Universal Serial Bus

Chapter 1

Introduction

1.1 Project Overview

Saliva sampling is an emerging diagnostic technique used as a non-invasive alternative to blood sampling. Capable of clinical identification of diabetes, inflammation, infections as well as hormonal perturbations [10], it has been increasingly used by researchers as part of routine dental and medical office examinations.

One possible application includes monitoring and balancing the pH of the mouth as a method to reduce bacteria causing tooth decay. Other studies have also been done to utilise the pH values of saliva as indicators of health conditions [11].

1.2 Device Brief

As mentioned previously, **the aim of this project would be to design a Smart Orthodontic Bracket (SOB) to be fitted in the mouth while monitoring the pH value of saliva.**

In order to achieve complete convenience for the user, the SOB should be maintenance free and be able to supply power as required. The pH data should also be easily accessible through an external device. Hence, **further specifications are for the sensor to be powered and communicated with through wireless techniques.** This SOB would serve as a tool for dentists to aid in monitoring their patient's dental health.

The project would entail 3 main phases: The **Design Phase, Prototyping Phase and Final Prototype Phase.** In the **Design Phase**, the design choices for each module in the SOB would be evaluated and justified. This involves the use of first a literature

Project Deliverables	
Phase	Deliverables
Design	(1) Define Specifications
	(2) pH Sensing Method
	(3) Determine Readout Circuit
	(4) Determine Energy Harvesting Module
	(5) Determine Wireless Communications Module
	(6) Design Circuitry for entire system
Prototyping	(7) Individual Modules
	(8) Overall Modules
	(9) Experimental PCB
Final Prototype	(10) Final Prototype PCB Design
	(11) Encapsulation of Device

TABLE 1.1: Project Deliverables

overview, with all plausible options considered. Next, components choices would be considered in regards to their specifications.

Once the design choices has been finalised, the **Prototyping Phase** would entail the implementation and testing of the separate components. Once tested up to pre-defined standards, the components would then be incorporated into a full, working device which would undergo further testing.

The **Final Prototype** phase would then consist of integrating the device into an orthodontic bracket. This would involve encapsulation of the device, as well as determining the optimum form of the bracket. **Table 1.1** shows the deliverables of the device for each phase.

The hardware deliverable would be the Smart Orthodontic Bracket, while software would involve code for programming the microcontroller. A phone app is used to power and communicate with the device.

1.3 Report Structure

The report structure would be based on the numerical order shown in **Table 1.1**. First, **Chapter 2** focuses on the medical background regarding orthodontic brackets, as well as the pH specifications, is done. Next, individual chapters from **Chapters 3,4 and 5** focusing on the research on pH sensing, energy harvesting as well as wireless communications is presented.

With the individual modules decided, **Chapter 6** would focus on the tests on each of the modules to ensure functionality. **Chapter 7** would then describe the tests done to

integrate these modules together. **Chapter 8** would entail the final prototype phase, with the encapsulation as well as the form of the final device decided upon, with an evaluation of its specifications. The work done is finally concluded in **Chapter 9**.

Chapter 2

Project Background

2.1 Medical Background

To validate the specifications of the pH sensor, an interview was conducted with a certified dentist, Dr Christine Mason [12] regarding the range of pH values to be expected, the form factor of the device, and the frequency of the readings required.

2.1.1 Form Factor



(A) Retainers with SOB attached to the side. As can be seen, the shape is slightly more freeform, as it is out of reach of the user's jaw motion. (B) Orthodontic Brackets, with SOB more narrow in order to avoid interfering with jaw motion. Taken from [13]

FIGURE 2.1: Proposed device fitting on different types of dental equipment

The key factor for the form would be **to avoid interference with the user's jaw motion**. Two possible methods for affixing the device exist - either through the use of retainers in [Figure 2.1a](#), or through the use of orthodontic brackets in [Figure 2.1b](#).

For a retainer that affixes to the jaw, the shape is slightly more freeform as compared to the bracket method. As the device can extend out towards the side of the mouth, this allows it to avoid the jaw motion completely.

For fitting of a bracket, the device will be glued to multiple back teeth in order to be affixed to the mouth. A limitation of this method is that the device must avoid interfering with the jaw motion of the user, and hence the form of the device has to be long and narrow to be below the teeth line.

This then has to be encased in a biocompatible material, of which two existing materials in use today are acrylic plastic and ceramic. The choice of the material will depend on its mouldability and flexibility, such that it can successfully encase the device made.

From this, two specifications are gathered. **The size of the device will be approximately less than 4cm, and it has to be biocompatible.**

2.1.2 Range of pH values and Frequency of Readings

The pH value of saliva in the mouth follows a baseline pH which varies in the range of [7, 7.5] for a healthy person[14]. 20 minutes after drinking an acidic substance(an example being wine), the pH level of saliva drops to acidic levels below 5. This would then revert back to the baseline pH after approximately 60 minutes.

When this baseline pH occurs at a low level, in the ranges of [5,7], is when there is a danger of the patient contracting tooth decay. This could occur due to teeth enamel issues, or silent gastric reflux, where acid from the stomach flows back up into the mouth.

The aim of the device would hence be to monitor these baseline pH values as required. This is expected to be **in the range of [5,8]**, and the precision required would be measurements at a single decimal place. The frequency is also dependent on the user, and would most likely be an hour after eating, or just after waking up.

These values are taken into consideration during the design phase of the project.

2.2 Prior Research

In this section, a review into the different methods available for the design of the pH sensor is given. Existing research on wireless pH monitoring, as well as pH monitoring in the mouth would be detailed. The research done would give rise to an envisioned high level design for the SOB.

Although wireless pH sensors exist commercially [15] [16], these are not meant for in-vivo usage due to their large sizes. Thus, research was done into non-commercial options available regarding wireless passive sensing for pH, as well as in-mouth measurements of pH values. Three papers were particularly useful to this topic.

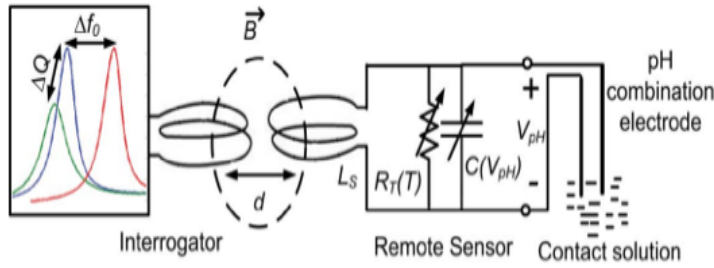


FIGURE 2.2: Block Diagram of IrOx electrode implemented circuit. Taken from [1]

Research conducted by the University of Manitoba in Canada included the implementation of a wireless passive pH sensor for temperature compensated remote monitoring [1]. In this application, an iridium oxide (IrOx) electrode and a silver chloride (AgCl) reference electrode was used in tandem with a Resistor-Inductor-Capacitor (RLC) coil resonator. The pH value varied the voltage across the electrodes, which caused a proportional change in the resonant frequency of the RLC coil resonator. This change in resonant frequency was then determined from an interrogator coil that transmitted power to the circuit at a frequency of 18MHz. This entire system is illustrated in **Figure 2.2**. This implemented sensor involved minimal use of integrated circuits (ICs), and was built with passive components as shown in **Figure 2.3**. The entire sensor was mounted on a single sided printed circuit board (PCB) of 4cm x 3cm. This made the size quite compatible with the project at hand, as can be seen in **Figure 2.3**.

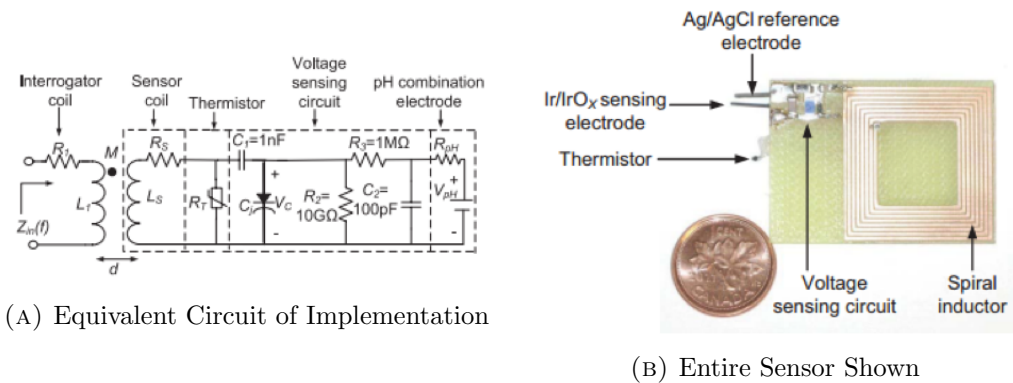


FIGURE 2.3: IrOx Electrode Sensing Circuit. Taken from [1].

The results from this paper were useful in directing the project, as it **provided a tried and proven method for pH sensing**. However, one of the limitations of this project was **the interrogator coil required for the powering of the device**. The coil had to be specifically manufactured, as well as being particularly large, and would be inconvenient for a patient to obtain or carry around. Furthermore, the frequency applied(18Mhz) is not in the ISM band range(covered further in **Section 4.4.4**), and hence would not be allowed for any commercial purposes.

The second paper involved the use of colorimetric detection of the pH using a smartphone based accessory manufactured as a smartphone case [17]. In this paper, a test strip containing the user's saliva is inserted into the optical system integrated into the smartphone case. Through the application of colour reagents, the pH of the solution could be detected. This paper **displayed the possibilities of pH sensing in relation to the mobile healthcare industry**, and will be explored in further detail when determining the frequency of transmission chosen for the wireless transmission design.

The last paper displayed research on in-mouth measurements of pH conducted by the University of Nottingham on the pH values of saliva while a subject was eating [18]. Their experimental set-up involved the use of a micro pH electrode embedded into dentures, which required an external power supply. In this paper, the sensor was noted to have a slight delay before obtaining measurements. This was also another factor in the type of pH sensing method chosen.

2.3 Detailed Specifications

The information gathered from Dr Mason and previous research is used to provide finalised specifications for the SOB as shown in **Table 2.1**.

Finalised Specifications	
No.	Specification
1	Read pH in the range of 5-8
2	Size of less than 3x3cm for fitting in mouth
3	Transmit Data Wirelessly
4	Obtain Power Wirelessly
5	Biocompatibility

TABLE 2.1: Detailed Specifications for SOB

These specifications would be used in the design of the SOB moving forward.

2.4 High Level Design

The background on in-mouth pH sensing was used to design an initial high level design for the SOB. The entire system is envisioned to consist of the following modules: the pH sensor, the read-out circuit, a microcontroller, the wireless data transmitter as well as the energy harvesting module. For non-SOB devices, the modules required would be a wireless data receiver, as well as a power transmitter module. This is illustrated in **Figure 2.4**.

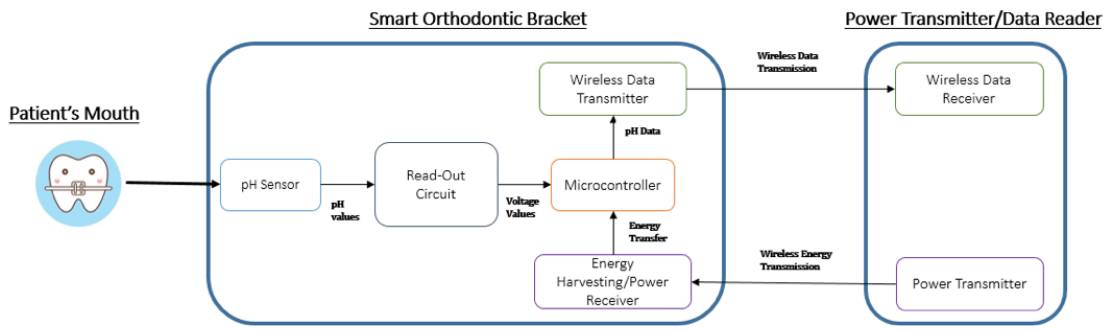


FIGURE 2.4: Overall Envisioned System of Smart Orthodontic Bracket (SOB) with required modules

The design decision for the modules will be prioritised in the following order:

1. pH Sensing Method
2. Read-Out Circuit
3. Energy Harvesting
4. Wireless Data Transmission

The rationale behind this is due to the overall requirements for the form factor of the device to be placed in the mouth. Hence, the pH sensor is the critical component, with the read out circuit being determined based on the pH sensor. The energy harvesting module is then chosen based on the power supply required for the sensing method. Lastly, the wireless communications module will be chosen based on the possible energy available to be harvested, or chosen based on the power transmission method.

Chapter 3

pH Sensing

3.1 Theory

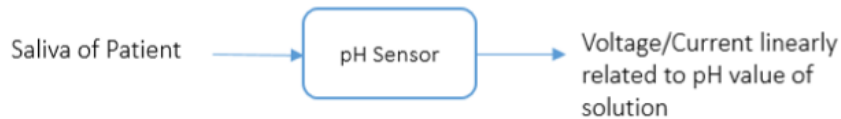


FIGURE 3.1: pH sensor module with required inputs and outputs

The pH sensing module input and output requirements is shown in **Figure 3.1** above. The pH is a value that is used to determine the acidity or alkalinity of a solution based on a scale from 0 to 14. A pH value of 7 indicates neutrality, while 0-6 indicates acidity and 8-14 indicating alkalinity. As mentioned previously in **Section 1.1**, the pH of biomarkers in saliva could be used to detect diseases in patients.

The pH is calculated based on **Equation 3.1**:

$$pH = -\log_{10} H^+ \quad (3.1)$$

Where H^+ is the molar concentration of hydrogen ions. A common method of measuring the pH is through the use of a combination electrode, which consists of a sensing and reference electrode. In this method, the potential of the sensing electrode would vary according to the pH value of the solution, while the reference electrode would remain at a constant potential. Thus, the potential difference across both electrodes, V_{pH} , would vary according to the Nernst Equation for combination electrodes in **Equation 3.2**:

$$V_{pH} = V_o - \frac{23026RT}{nF} pH \quad (3.2)$$

Where V_o is related to the potential at the reference electrode, R is the Gas Law constant, T is the temperature in Kelvin, n is the stoichiometric number of ions, and F is Faraday's constant. As shown from the variable T , this gives rise to possible temperature drift in the sensors as seen in [16] and [18]. Most of the methods looked at are different forms of combination electrodes, which will apply to **Equation 3.2** above to obtain a pH value.

3.2 Requirements for Module

The requirements for the pH sensor of the device are the following:

1. **Biocompatibility** : For the sensor to be in contact with human fluids without medical issues, since the sensor is the only part of the SOB in contact with the patient.
2. **Size** : For the sensor to be of a reasonable size for retro-fitting in the mouth, to be less than a length of 4cm.
3. **Read Out Circuit** : Whether the sensor requires additional components for a read out circuit, or if it is already integrated.

3.3 Analysis of Options

4 different pH sensor types were evaluated. The glass electrode, Ion-Sensitive Field Effect Transistor (ISFETs), Iridium Oxide electrodes as well as fibre-optic methods.

3.3.1 Glass Electrodes

The glass electrode sensor [2] works by comparing a voltage across a glass membrane, with a reference pH solution internal to the glass membrane and the test solution external to the glass membrane. The voltage value determined would give an indication of the pH value of the test solution. This is illustrated in **Figure 3.2** above.

The main advantage of this method was that it was the most common measuring method, with almost all probes found commercially consisting of glass electrodes. Hence, implementation of glass electrodes would be the most straightforward in comparison to other pH sensing methods. The other advantages were that there was no temperature dependence for pH sensing acidic compounds.

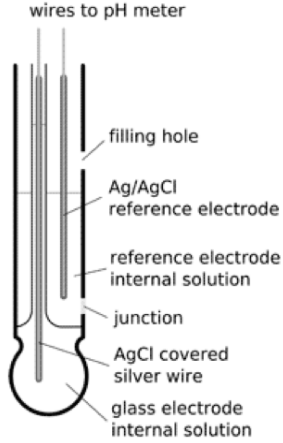


FIGURE 3.2: Glass Electrode Configuration. Taken from [2]

However, this method was unable to fulfil the form factor, with the smallest glass electrodes found commercially, micro pH electrodes from Sigma-Aldrich [19], having an electrode length of 183mm. This made it unsuitable for use in the mouth. Furthermore, the cost of the glass electrodes (£280 for [19]) were generally quite high.

3.3.2 Ion-Sensitive Field Effect Transistors(ISFETS)

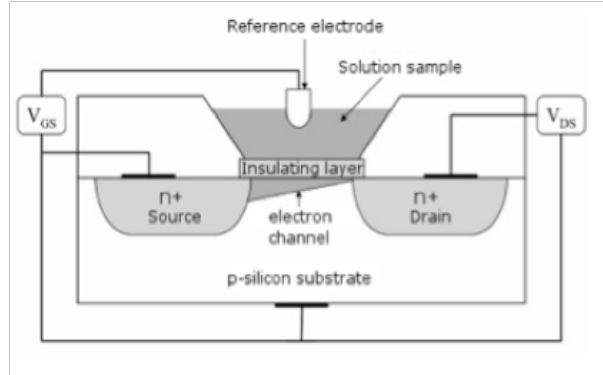


FIGURE 3.3: ISFET Diagram

ISFETs contain an ion-sensitive layer between the gate and bulk, as opposed to a normal insulating layer, usually SiO_2 , in a conventional MOSFET. By varying the ion concentration around the ion-sensitive layer, the threshold voltage of the transistor changes. An example circuit is shown in the figure above. By keeping the gate voltage constant with a reference electrode, a change in the ion concentration sample would induce a change in the current flowing through the circuit. This current could be measured with an accurate amperometer to determine the pH level. However, it has to be noted that ISFET sensors are not commercial, and have to be specifically fabricated. The sample

applied in this case is obtained from the Centre of Bio-Inspired Technology (CBIT) [20], with the fabrication method described in this paper [21].

The advantages of an ISFET based pH sensor is the size. As shown from the above example, the size of the sensing array is 0.7mm x 0.4mm, while the read out IC for the current has an area of 0.6mm². Hence, the form factor is extremely ideal for our application. The power requirements for the chip is considerably low as well for use in wireless applications (9.9mW). This sensor also consisted of a read-out IC, which reduced the complexity required since the read-out IC had been designed.

However, one of the issues faced with this is biocompatibility of the ISFETs. The ISFETs are manufactured using complementary metal-oxide-semiconductor (CMOS) technology, with aluminium involved in the process. As aluminium is a reactive metal that will corrode in the presence of saliva, this would cause severe irritation to human tissue.

3.3.3 Iridium Oxide(IrOx) Electrodes

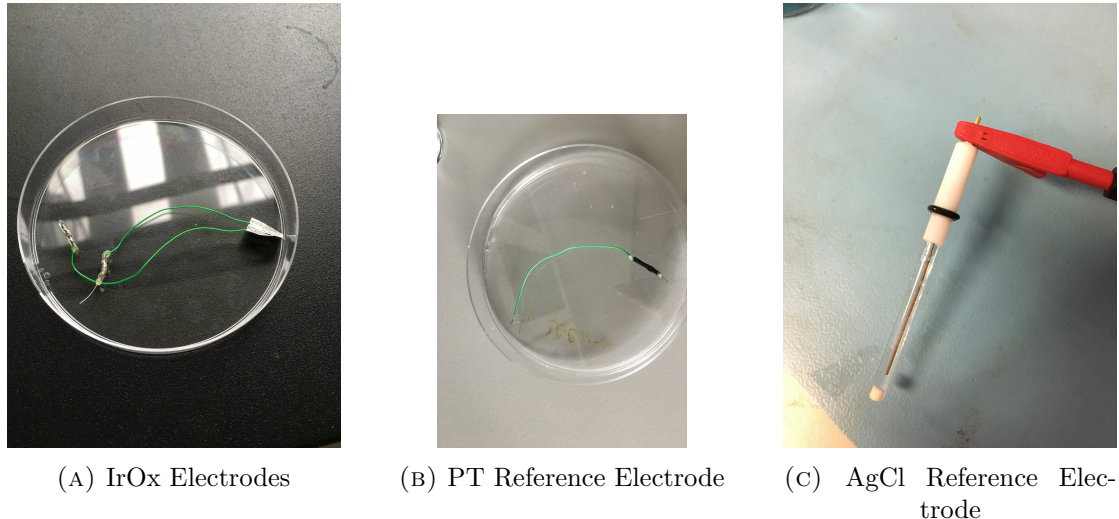


FIGURE 3.4: Different Electrodes used for pH sensing

Iridium Oxide(IrOx) electrodes are a type of metal oxide electrode with a pH dependent potential. By comparing this potential to a reference electrode that is independent of the pH, the potential difference between these two electrodes could be used to determine the pH of the solution. The IrOx electrode is fabricated from CBIT[22], and is unavailable commercially. This method is proven to work as shown in [1].

The advantages of this combination electrode would be its small size, IrOx electrode simply being a single strip of wire. It is also biocompatible with the human body since IrOx does not corrode in bio liquids, and hence it would be able to come into contact with saliva.

The reference electrode in this case are silver chloride(AgCl) glass electrodes from Sigma Aldrich [23]. The AgCl electrode did not come in a small package, and hence another option was provided for the reference electrodes in the form of platinum(Pt) cuffs. All the electrodes can be observed in **Figure 3.4**.

The disadvantage of this method would be that a read out circuit would have to be implemented for the electrodes. This introduces another layer of complexity to the pH sensing method.

3.3.4 Fibre-Optics

The last method looked into was fibre-optic pH sensors. Colour indicators are used on the measured solution which turn the pH to a certain colour. This could be used visually for a rough method of estimating the pH. For a more precise method, a light source with a photodetector is used to improve the accuracy [24][25]. This method is also used in the Smartphone accessory implementation done in [17].

The advantages of this method is its small form, with the sensor capable of being placed in the mouth. However, this method would only work with transparent liquids, as well as requiring a large power supply for the light source and photodetector. The largest disadvantage was the size of the optical sensor required for detection of the pH.

3.4 Choice of Method

Table 3.1 displays the various pH sensing methods, along with an evaluation into their advantages and disadvantages with respect to the requirements above.

pH Sensing Method	Bio-compatibility	Size	Read Out Circuit	Source
Glass Electrode	Yes	Large	Not Required	[19][26]
Ion-Sensitive Field Effect Transistors(ISFETS)	No	Small	Not Required	[21]
Iridium Oxide	Yes	Small	Required	[1][22]
Fibre-Optics	Yes	Large	Required	[24][25][17]

TABLE 3.1: pH Sensing Options

The choice of the sensing method was through the use of **iridium oxide electrodes**. With the choice of this electrode, the biocompatibility and size requirements for the SOB is fulfilled. This method was the only viable method, as all other methods were unable to fulfil size or biocompatibility requirements. However, this method requires the design of a read-out circuit to be used with the electrodes. This will be done in **Section 3.5**.

3.5 Readout Circuit

With the implementation of IrOx electrodes, a read out circuit with the following inputs and outputs is required as illustrated in **Figure 3.5** below.

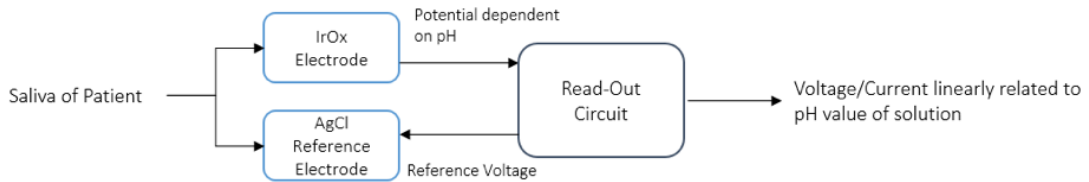


FIGURE 3.5: Iridium Oxide Electrodes with Read Out Circuit

In order to read the voltage values from the IrOx electrode, a way of holding the output voltage stable for a microcontroller's ADCs to read is required. Similarly, a stable reference voltage is required for the reference electrode in order for a stable comparison to the potential from the IrOx electrode. Thus, the circuit required would involve two voltage buffers with negative feedback applied, to ensure that the reference electrode would obtain a stable voltage reference, and the sensed voltage would have a stable output. This is shown from the circuit below in **Figure 3.6**.

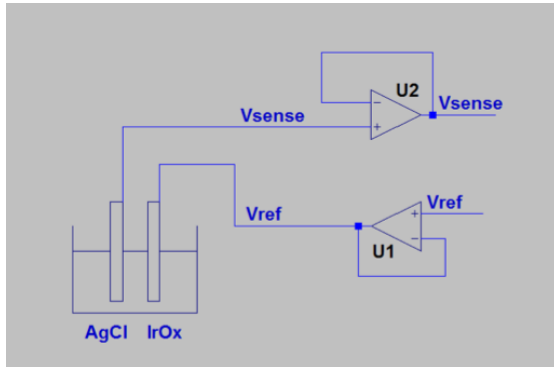


FIGURE 3.6: Iridium Oxide Electrode Proposed Read-Out Circuit

In order to integrate this circuit, a number of ICs were compared. The first criteria was for low power dual op amp ICs, from which there were many examples to choose from. The OP290 [27] from Analog Devices, LM series from Texas Instruments [28], as well as the LT112 from Linear Technology [29]. The eventual IC chosen was the LMP91200 from Texas Instruments [30], due to its advantages of being optimised for low-power applications, as well as being specific for pH sensing applications. However, its main advantage was the in-built potential divider, which allowed the same VCC to be applied at the input and immediately halved for a reference voltage output. An example implementation for the LMP91200 is also found for a wireless sensor transmitter, albeit for industrial applications [31]. The LMP91200 setup is shown in **Figure 3.7**.

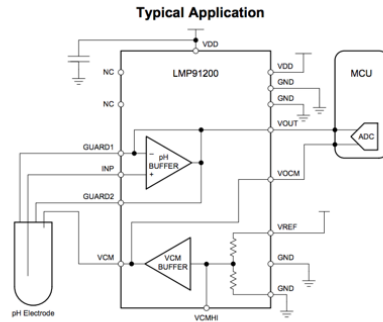


FIGURE 3.7: LMP91200 pH Sensing IC

The key components of this circuit are:

1. The pH buffer, a unity gain buffer used to read the electrode voltage.
2. Common-Mode Voltage Buffer, used to supply the reference voltage.
3. Comparison of VOUT and VO CM, which is the differential voltage used for determining the pH.
4. The availability of an in-built potential divider to the VREF output, which relieves the need for external resistors for providing a reference voltage.

The supply voltage for this IC is 1.8V to 5.5V, and the supply current is 50 μ A. For a 3.3V supply, the estimated power requirement is about **165 μ W**. Hence, this IC runs at extremely low power, as well as having a size (5mmx4mm) that is ideal for placement in the mouth.

3.6 Chapter Summary

The choice of pH sensing is determined in this chapter as IrO_x electrodes. In addition to this, a readout circuit for these electrodes is designed. The LMP91200 will be used to implement this circuit due to its low power(165 μ W), and the internal potential divider which alleviates the need for external resistors.

Chapter 4

Energy Harvesting

The aim of the energy harvesting module is to supply energy to the entire system. The requirements for the module are that it has to power the pH sensor and the read out IC required. At the same time, it also has to power the wireless communications required, as well as the microcontroller. Hence, in regards to this, it is critical that the minimum power that the power supply module can supply is more than 1mW.

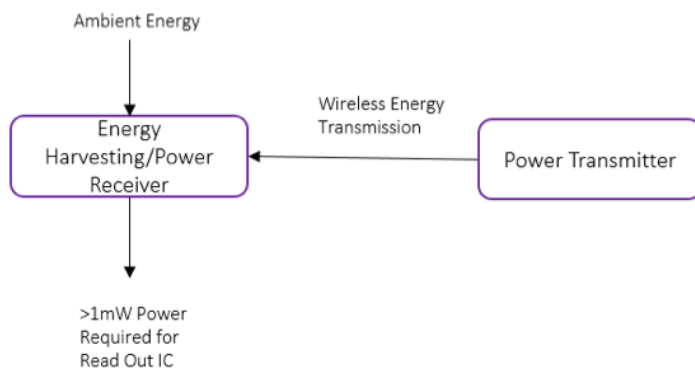


FIGURE 4.1: Energy Harvesting Module

The overall module is illustrated in **Figure 4.1** above. In order to better understand the different methods of powering biosensors wirelessly, research is done on wireless powering of bio-sensors. This will be separated into physical energy harvesting and radio frequency(RF) energy harvesting.

4.1 Physical Energy Harvesting

Physical energy harvesting is a technique whereby energy is scavenged from external sources such as heat or motion. In this case for a sensor placed in the mouth, the

possible sources of energy would be through the heat from the mouth, as well as the jaw motion of the user.

4.1.1 Thermoelectric Harvesting

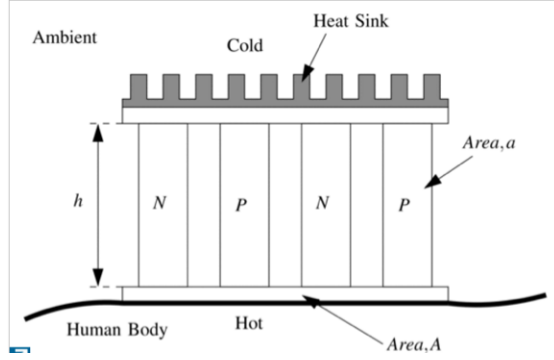


FIGURE 4.2: Illustration of Thermoelectric Harvesting from a user's body. Taken from [3]

In order to utilise the possible heat generated from the mouth, a thermal gradient is required across two different metals, which creates a voltage drop across them. This voltage drop can then be used to provide energy to any components. This is illustrated in **Figure 4.2**, and a number of implementations are explored in [32][33][34].

The limitations are that the power ranges for such devices are limited to around 30uW to date [5]. Furthermore, a heat sink would be required for a thermal gradient, which may entail the energy harvesting device in the mouth having to be connected to a heat sink outside the mouth. This would make the device unwieldy, and hence this method would not be reliable as a primary source of power.

4.1.2 Motion Harvesting

The other harvesting technique considered was harvesting the jaw motion of a user. This method would involve the use of piezoelectric materials or electrostatic transducers to produce energy from motion. Example implementations are described in [3], where motion harvesting methods are evaluated.

The limitations for this method were that the possible power from available commercial sources were limited to $80/\mu\text{W}$ [5]. This was due to the maximum power being limited to the size of the sensor, as well as the frequency of the motion [35]. With the frequency of the jaw motion being inconsistent, as well as being particularly low(less than 1Hz), this method was not considered to be viable as the primary source of the power supply.

4.2 RF Energy Harvesting

RF energy harvesting involves the transmission of power from a source to a load without any interconnecting conductors. Different wireless power techniques exist, though the two main plausible methods for wireless powering are infrared radiation and inductive coupling, due to the ability of these methods to transmit power through skin.

4.2.1 Infrared Radiation

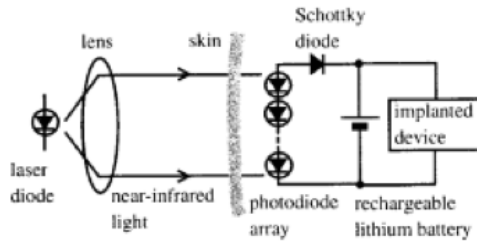


FIGURE 4.3: IR Harvester Circuit Implementation. Taken from [4]

Infrared Radiation (IR) is a method where an external IR source is used to transmit power to an in-vivo photodiode array. The possible received power is up to 4mW [5]. The limitation of this method is that tissues in between the source and the load would cause a rise in temperature. Increasing the transmitter power would cause the temperature of the implantation zone to rise, and would make it unsuitable for uses in the mouth. However, at the required power of 1mW, this method might be utilised for power transmission.

4.2.2 Electromagnetic Inductive Coupling

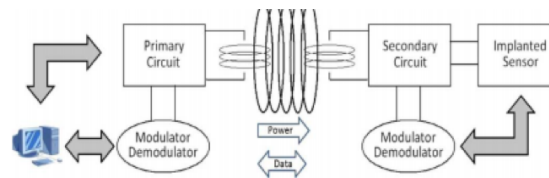


FIGURE 4.4: Inductive Coupling with Power and Data Transmission. Taken from [5]

This method of wireless power transfer involves the use of electromagnetic induction for wireless power transfer. A transmitter coil outside of the body is used to generate an alternating magnetic field through an alternating current flow. As the current flows through this transmitter coil, an alternating magnetic field is generated. When this alternating magnetic field passes through the receiver coil for the implanted sensor, a voltage is induced as per Lenz's Law:

Energy Harvesting Method	Power > 1mW	Form	Source
Thermoelectric Harvesting	No	No	[32][33][34]
Motion Harvesting	No	No	[3][5][35]
Infrared Radiation	Yes	No	[5]
Inductive Coupling	Yes	Yes	[36][37][38][39]

TABLE 4.1: Evaluation of Energy Harvesting Methods

$$\varepsilon = -\frac{d\phi_B}{dt} \quad (4.1)$$

Where ε is the induced voltage, and ϕ_B is the magnetic flux through the transmitter coil.

Inductive coupling can be used to transmit power wirelessly in the range of 10 – 90mW [36][37][38][39]. This method seemed the most reliable in terms of power transfer, as well as having extensive research proving its viability.

4.3 Analysis of Options

Evaluation of the methods for the energy harvesting module in **Table 4.1** shows that the physical energy harvesting solutions to be of insufficient power. One option is to pair them with supercapacitors in order to store the energy required. However, another issue was with the physical form of the methods. For thermoelectric harvesting, a cold sink needs to be placed outside the mouth for a difference in temperature. This would be unsuitable for the form of the SOB. On the other hand, the low frequency of jaw motion, as well as its inconsistency, would lead to a poor power generation. Hence, the decision was made to research further into inductive coupling as a method of supplying power. This would be done in **Section 4.4**.

4.4 Inductive Coupling

As inductive coupling can occur across a range of frequencies, it is imperative to determine the optimum frequency for the SOB. There are a number of factors that determine the frequency used for inductive coupling. The theory behind inductive coupling is required in order to provide a justification into the optimum frequency for transmission, given an estimated receiver coil size.

4.4.1 Antenna Sizes and Energy Transmitted

Generally, the transmission frequency for inductive power transfer varies in the radio frequency range of 3Hz -3000GHz. The frequency is given by [Equation 4.2](#):

$$f = \frac{c}{\lambda} = \frac{E}{h} \quad (4.2)$$

Where c is the speed of light, λ is the wavelength, E is the photon energy and h is Planck's constant. Hence, it can be observed that the frequency of the wave is inversely proportional to the wavelength and proportional to the energy ($f \propto \frac{1}{\lambda} \propto E$). For efficient transmission, the antenna length should be at least a quarter of the wavelength transmitted. This means that **smaller antennas could be applied at higher frequencies**, which would fit well into the form factor of the SOB. Furthermore, the power supplied increases at higher frequencies.

4.4.2 Penetration Depth

Another important factor in determining the frequency would also be the penetration depth. The penetration depth measures the distance an EM wave can penetrate into a material, and occurs when the intensity of the radiation falls to $\frac{1}{e}$ of its original value. Considering that the SOB would be in the mouth, the power transferred would be through a layer of biological tissue. Thus, the degree of decay of the EM wave through tissue would be significant in this study. The depth of penetration is given by the following formula [\[40\]](#):

$$\text{Depth of Penetration} = \frac{1}{2\pi f} \left[\frac{\mu\epsilon}{2} \left(\sqrt{1 + \left(\frac{\sigma}{\epsilon 2\pi f} \right)^2} - 1 \right) \right]^{-\frac{1}{2}} \quad (4.3)$$

Where f is the frequency of the radiation, μ is the permeability of the material, ϵ is the permittivity of the material, and σ is the conductivity of the material. Hence, as the penetration depth is inversely proportional to the frequency of transmission ($\text{Depth of Penetration} \propto \frac{1}{f}$), it can be stated that **lower frequencies increase the transmission efficiency**.

4.4.3 Alternative Viewpoints

A recent paper into the optimal frequency for wireless power transmission into dispersive tissue disputes **Equation 4.3** [41]. In this paper by the Department of Electrical Engineering in Stanford University, the rationale behind using a low-frequency carrier for wireless power transmission omits displacement current. In that case, the electromagnetic field propagation diffusion equation is a quasi-static approximation to Maxwell's Equations. Solving this equation yields that the electromagnetic field decays as frequency increases, as shown in **Equation 4.3**. Thus, most of the studies tend to involve the use of frequencies below 10 MHz for wireless power transfer.

By modelling tissue as a low loss dielectric with significant displacement current, a Helmholtz equation could be used. Solving this would reveal that **penetration depth is independent of frequency at higher frequencies**. Thus, a higher frequency could be used for transmission into skin without a loss of efficiency.

The optimal frequency for maximum power transmission could be calculated based on modelling biological tissue as a dispersive dielectric in a homogeneous medium. From [41], the optimal frequency for maximum power transmission would then be:

$$f_{opt} \approx \frac{1}{2\pi} \sqrt{\frac{c\sqrt{\epsilon_r}}{d\tau(\epsilon_r - \epsilon_\infty)}} \quad (4.4)$$

Where d is the transmit-receive distance, c is the speed of light and τ , ϵ_r and ϵ_∞ are dielectric properties of the tissue in the Debye relaxation model. Based on the measured values of the dielectric properties in [42], the optimum frequency through wet skin for a distance of 5cm is approximately 3GHz. The closest ISM band to this is 2.4 GHz.

4.4.4 Industrial, Scientific and Medical(ISM) Radio Bands

The last factor for determining the frequency are ISM bands, which are frequency bands in the radio frequency range reserved for industrial, scientific and medical uses. These bands limit the usage of frequencies to a certain range, such as to limit interference from other applications. In order to comply with international regulations, these ranges must be used.

4.5 Choice of Frequency

The research done showed a possible discrepancy for the determination of the optimal frequency, and that any mathematical equations were unlikely to yield a clear optimum. Thus, the next best method was to rely on simulations to simulate an electromagnetic field and observe its effects on skin. The high frequency structural simulator(HFSS) software from ANSYS[43] is an industry standard software used for the simulation of such fields to determine the power transfer across a medium. However, the use of this simulation tool was deemed beyond the scope of the project, and instead the decision was made to look at current commercial options for comparisons. HFSS would possibly be explored in future work.

In lieu of this, the research approach was modified in order to determine available energy harvesting ICs on the market that could fit the form, as well as power requirements for the SOB. The available components were based on the ISM bands, and consisted of 2 frequencies: 915Mhz and 13.56Mhz.

4.6 Options for RF Energy Harvesting ICs

IC	Frequency(MHz)	Size(mm)	Output Voltage(V)	μ C	Transmitter	Source
P1110B	912	0.55x0.43	3.3/4.2	No	Proprietary	[44]
AS3955	13.56	2.125x1.42	1.8-4.5	No	NFC-Enabled Device	[45]
RF430FRL152H	13.56	16x16	1.5/3	Yes	NFC-Enabled Device	[46]
SL900A	13.56	5x5	NA	Yes	NFC-Enabled Device	[6]

TABLE 4.2: Energy Harvesting IC Options

Table 4.2 describes the available commercial options for RF energy harvesting ICs. The PowerHarvester ICs from PowerCast appeared to be an excellent option, but it was noted that the frequency of transmission required a specific transmitter for power transmission that was large, and was unlikely for a patient to carry around.

Hence, this left the remaining options for a 13.56Mhz based transmission. The AS3955 had the smallest size, although the other two components contained inbuilt microcontrollers. However, the critical point was the comparison of the output voltage values. Given that the output voltage range of the AS3955 could be varied through software, as well as being able to supply 5mA@4.5V, this IC seemed the most logical choice for the SOB. An additional advantage was the availability of an AS3955 demokit which contained implementations of working tags with an Android app, which could be used to enhance the testing of the device.

Thus, the decision was made to **utilise the AS3955 as the energy harvesting IC**.

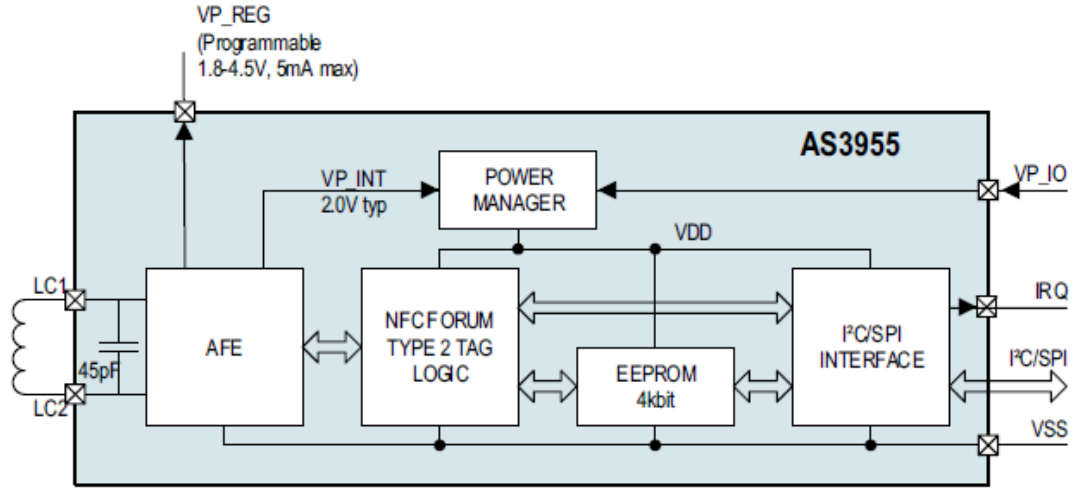


FIGURE 4.5: AS3955 Block Diagram. Taken from [6].

Figure 4.5 shows the block diagram of the AS3955. The key components in this IC are:

1. VP Reg, which provides a regulated voltage supply in the range of 1.8-4.5V
2. NFC Forum Type 2 Logic, which provides internal logic to modify modulated signals into a standardised NFC format
3. An EEPROM, which allows storage of information to be read by a reader
4. An I2C/SPI Interface, which allows for communications with a microcontroller
5. LC, an external antenna for energy harvesting, and NFC communications

As the AS3955 IC relies upon NFC for communications, this will be the chosen wireless communications method. NFC will be expanded further upon in **Chapter 5**.

4.7 Chapter Summary

The choice of the energy harvesting method would be through inductive coupling. This was chosen due to its capability of supplying at least 1mW of power. The AS3955 was picked among commercial energy harvesting IC options due to its functionality of having a variable voltage supply, as well as an EEPROM for data storage.

Chapter 5

Wireless Communication Module

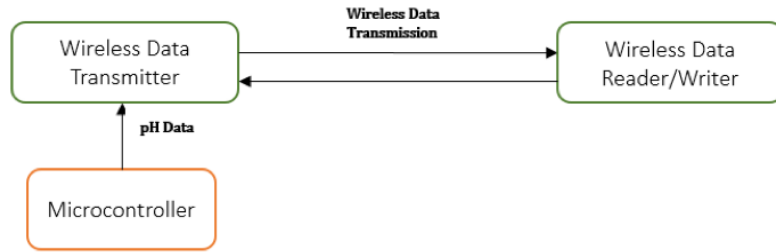


FIGURE 5.1: Wireless Communications Module

The aim of the wireless communication module is to send the pH data from the SOB to an external receiver. Given the choice of the AS3955 IC as the component used for the energy harvesting module, the determination of the wireless communications method was chosen to be the near field communication(NFC) protocol. Hence, this chapter would explain the theory behind the NFC protocols to aid in the understanding of the implementation and testing of the SOB. In addition to this, the antenna and microcontroller for communications with the AS3955 will be chosen in this chapter.

5.1 Near Field Communication(NFC)



FIGURE 5.2: Near Field Communication Protocol

NFC is a RF protocol used for communication between devices at a distance around the range of 10cm or less. The protocol applied by the AS3955 IC is covered by the ISO 4443A standard. As mentioned in [Section 4.6](#), this protocol is supported by Android operating system smartphones and tablets, while at the moment, developer access for Apple NFC is unsupported[47].

The terminology applied for NFC protocol devices is the *reader*, a device that contains a transmitter and usually initiates communication, and a *tag*, a device that is usually powered by the reader and contains information to be read by the reader.

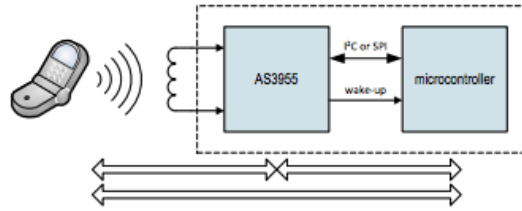


FIGURE 5.3: Reader and Tag System Diagram. Taken from [6].

[Figure 5.3](#) displays the system diagram for the AS3955 chip, where the reader in this case would be a smartphone, while the tag in this project would be considered the AS3955, with a microcontroller containing the data to be transmitted.

The standard specified by the ISO 4443A ensures that NFC operates in the 13.56Mhz band, and as mentioned in [Section 4.2.2](#), power is transferred from a reader to a tag through inductive coupling.

The AS3955 is capable of active or passive communication modes. Active mode indicates that the tag is powered externally by a power supply, and can possibly initiate communications with a reader. Passive mode indicates that the tag obtains power from the reader, before performing the required actions. For this project, the tag would be configured in passive mode. However, active mode would be used during debugging of the tag with power supplied from an external source.

5.1.1 NFC Methodology

As a tag enters the field of a reader, an AC voltage is applied across the antenna inputs. As seen in [Figure 5.4](#), this AC voltage applied is then passed through the **Rectifier** into a DC power supply for powering the chip. The **External Regulator** allows this applied voltage to be varied in the range of 1.8V-4.5V, while the current provided by this external regulator is determined by the reader field strength, antenna size and Q factor, which would be covered in [Section 5.2](#).

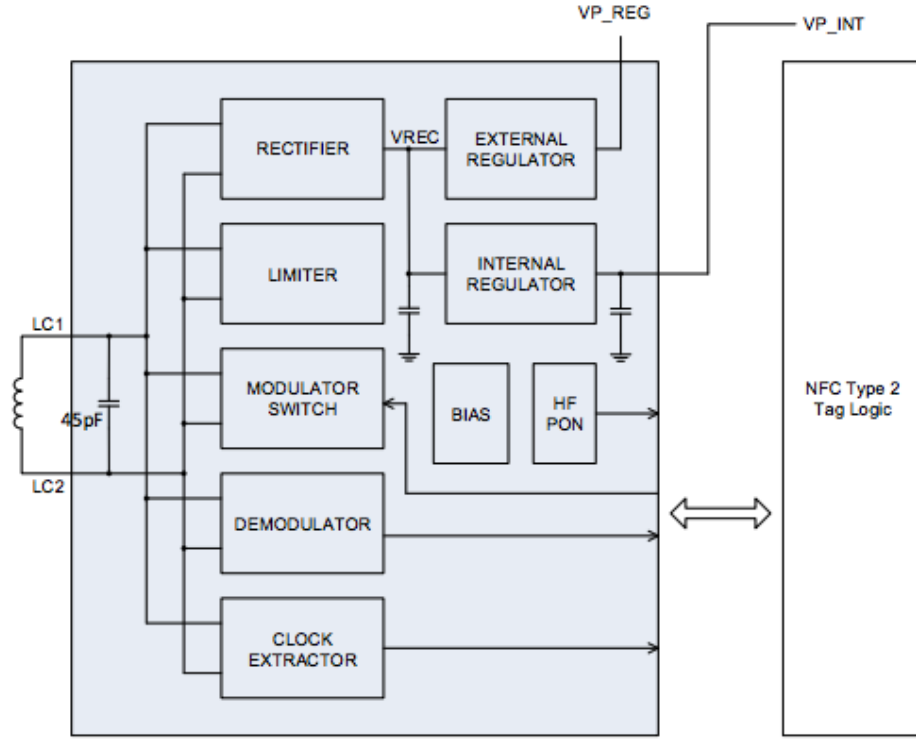


FIGURE 5.4: Analog Front End of AS3955 Chip. Taken from [6].

5.1.1.1 Modulation Schemes

There are two key modules for communication - the **Modulator Switch** and the **Demodulator**. To transmit data from the reader to the tag, amplitude shift keying(ASK) on the magnetic field is applied, which is detected by the **Demodulator** according to the ISO 4443 specifications. On the other hand, to transmit data from the tag to the reader, load modulation is applied. This is done by the **Modulator Switch**, where a load impedance is varied according to the data to be sent, varying the resonant state between the reader and the tag. This causes the reader's transmitter coil characteristics to vary, and demodulating this signal allows the data to be extracted[48][49].

5.1.1.2 NFC Forum Type 2 Tag Platform

Finally, the AS3955 contains the logic for NFC Forum Type 2 Tag communication. Instead of having to convert ASK and load modulated bits to understandable information, it uses the NFC Forum data format(NDEF) messages to have a **standardised data format across all NFC tags and readers**. This allows the advantage of being able to use any NFC Type 2 reader compatible with any NFC Type 2 tag.

Example NDEF Layout										
1 Byte	1-3 Bytes						...			
Type	Length	Value								

FIGURE 5.5: NDEF Message Block

The NDEF format is defined in **Figure 5.5**. It consists of three fields:

1. The **type** field, which indicates the type of the block.(0x03 for NDEF)
2. The **length** field, which indicates the size of the bytes in the value field. For a value field of 5, the value will be 0x05. This can go up till 65535 bytes.
3. The **value** field, which carries the data bytes.

This NDEF logic for converting NDEF messages to modulated data is handled by the AS3955, and hence transmitted signals to the tag would need to be in NDEF formats. This overall system for the AS3955 can be seen in **Figure 5.6**.



FIGURE 5.6: AS3955 with associated modules

The antenna design as well as the microcontroller would be chosen in the later sections.

5.1.2 Comparison with other existing protocols

The advantage of NFC over other wireless communication protocols such as Bluetooth Low Energy(BLE) and WIFI is its ability to power the device wirelessly. Furthermore, with the limited proximity of its communication(<10cm), it is far more secure in comparison to the other protocols in regards to the possibility of data theft.

It is also important to note that the communication range of NFC is fairly limited by the distance and data rate(10cm, 424kbits/s) as compared to WIFI(100m, 600Mbps) and BLE(50m, 1Mbps). However, for the purpose of data transfer of the SOB, the data rate

and distance are not key factors to the wireless communication as mentioned previously in the specifications. In fact, with the proliferation of smartphones, it is seen as an advantage for the use of NFC to communicate data due to the availability of readers for power transfer. This removes the need to buy or build special readers that transmit at certain frequencies.

5.2 Antenna

As the antenna is not included as part of the AS3955 IC package, and considering that the antenna plays a role in the amount of power obtained by the tag itself, the fundamentals behind an NFC antenna are given to explain the rationale behind the design[50].

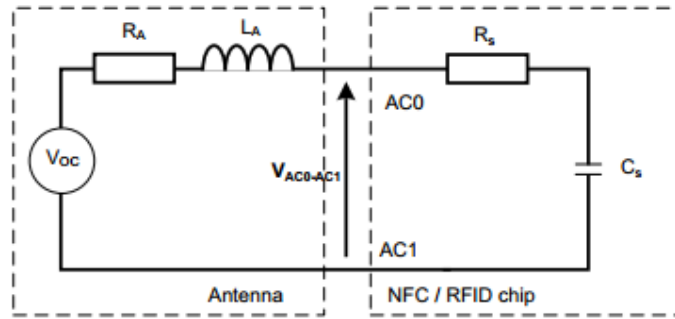


FIGURE 5.7: Equivalent Circuit Model of an NFC tag in the presence of a field. Taken from [7].

Figure 5.7 shows the equivalent circuit model of an NFC tag with its antenna in a generated field. The parameters include:

1. V_{OC} , the open circuit voltage generated by the antenna. It is dependent on the magnetic field strength, antenna size and number of turns of the antenna.
2. L_A , the equivalent inductance where $L_A = \frac{\text{Antenna Reactance}(X_A)}{2\pi f}$
3. R_S , the equivalent power consumption of the NFC chip and R_A , the equivalent antenna resistance
4. C_S , the equivalent serial tuning capacitance of the NFC chip, 45pF in the case of the AS3955

At resonant frequency(13.56MHz), the antenna impedance is given by:

$$Z_{ant} = R_A + jL_A(2\pi f) \quad (5.1)$$

while the NFC chip impedance is given by:

$$Z_{IC} = R_S + j\frac{1}{C_S 2\pi f} \quad (5.2)$$

In order to maximise the current and the voltage, the total impedance $Z_{ant} + Z_{IC}$ must be at a minimum. This occurs at resonant frequency, where $L_A C_S (2\pi f)^2 = 1$. Substituting this equation into **Equations 5.1 and 5.2** yields the final equation, $Z_{Total} = R_A + R_S$. The total impedance is now minimal, as compared to when inductive or capacitive impedance is introduced. Hence, the current and voltage delivered to the chip is maximised, and power is at a maximum.

5.2.1 AS3955 Required Antenna Inductance

Referring back to **Figure 5.4**, it can be observed that the antenna inputs LC1 and LC2 form a parallel LC circuit with the 45pF capacitor. This 45pF capacitor is required to resonate at a frequency of 13.56Mhz, which allows us to calculate a theoretical optimum for the antenna inductance. The resonant frequency of a parallel LC circuit is given by **Equation 5.3**.

$$\text{Resonant Frequency} = \omega_0 = \frac{1}{\sqrt{LC}} \quad (5.3)$$

Substituting in the values for the capacitor, C , and the frequency, $f = 13.56MHz$, we obtain the following inductor value in **Equation 5.4**.

$$L = \frac{1}{(2\pi f)^2 C} = \frac{1}{(2\pi(13.56 \times 10^6))^2 \times (45 \times 10^{-12})} = 3.061\mu H \quad (5.4)$$

This would allow us to determine an approximate optimal value for the inductor used as the antenna inputs to be $3.061\mu H$.

5.2.2 Obtaining the antenna

In order to obtain a $3.061\mu H$ antenna, two routes were chosen. The first route was to find available commercial antennas and test them with the set-up, while the second route was to design PCB antennas for accurate inductance matching.

5.2.2.1 Commercially Available Antennas

A number of 13.56 Mhz-operating antennas were sourced from Digikey, and were used to test with the NFC chip. Most of the antennas came from Abracon's ANFCA Series[51]. Only antennas below the size range of 40mm were chosen. The antennas tested can be found in **Table 5.1** below.

Antennas	Inductances(μH)	Size(mm)	Source
W7001	0.9	25x25	[52]
ANFCA-3225-A02	1.8	32x25	[53]
ANFCA-1510-A02	1.8	15x10	[54]
ANFCA-2515-A02	1.8	25x15	[55]
ANFCA-2525-A02	1.8	25x25	[56]

TABLE 5.1: Commercial NFC Antenna Options

As seen above, the antenna values of $1.8\mu\text{H}$ is not the optimal inductance required for the LC tank for the AS3955 AFE. Hence, capacitive compensation was applied.

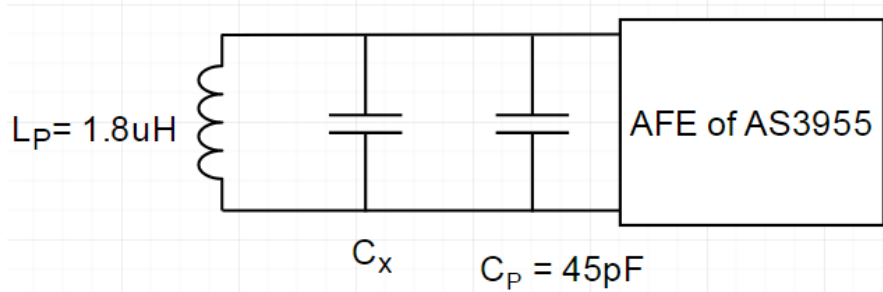


FIGURE 5.8: Capacitive Compensation for NFC antennas

Figure 5.8 describes the capacitive compensation required for an inductor of $1.8\mu\text{H}$. For this case, the resonant frequency in **Equation 5.3** is modified as shown in **Equation 5.5**.

$$\text{Resonant Frequency} = \omega_0 = \frac{1}{\sqrt{L(C_X + C_P)}} \quad (5.5)$$

Where the new parameter is C_X , the capacitive compensation applied. For the case of an inductor with a value of $1.8\mu\text{H}$, the value of C_X can be calculated as shown in **Equation 5.6**.

$$\begin{aligned} C_X &= \frac{1}{(2\pi f)^2 L} - C_P = \frac{1}{(2\pi(13.56 \times 10^6))^2 \times (1.8 \times 10^{-6})} - (45 \times 10^{-12}) \\ &= 3.153 \times 10^{-11} F = 315nF \end{aligned} \quad (5.6)$$

This equation was used to calculate the required capacitive compensation for the tests with the external antennas later in **Chapter 6**.

5.2.2.2 Designing the Antenna

To design the antenna, it was important to source the equation for the inductance of a rectangular loop antenna. This was obtained from [7], where **Figure 5.9** shows the rectangular loop coil to be implemented, and the inductance of the rectangular loop coil in **Equation 5.7**.

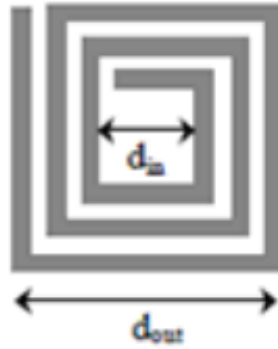


FIGURE 5.9: Rectangular Loop Coil. Taken from [7].

$$L_{ant} = 2.34 \times \mu_0 \times N^2 \times \frac{\frac{d_{out}+d_{in}}{2}}{1 + 2.75(\frac{d_{out}-d_{in}}{d_{out}+d_{in}})} \quad (5.7)$$

To further aid in the accuracy of the antenna design, a Panasonic NFC Antenna Online Tool[8] was used to ensure the inductance was accurate. In this tool, the parameters such as the width, height, gap, thickness of the copper as well as the number of turns could be varied in order to obtain the desired inductance. In addition, the antenna gerber data could be output from the software in order to be used in the PCB design. The software interface can be seen in **Figure 5.10**.

This tool was then used to design 4 antennas. The first three antennas varied around the optimal inductance value of $3.061\mu\text{H}$, while the last antenna varied in form while having the optimal inductance value. These antennas can be seen in **Figure 5.11**. The designed antennas parameters are assigned in the figure, with Y and X indicating their height and width, while W indicates the track width, g the spacing between the tracks, t the thickness of the copper and N indicating the number of turns of the antenna.

These antennas would later be used for tests in **Chapter 7**.

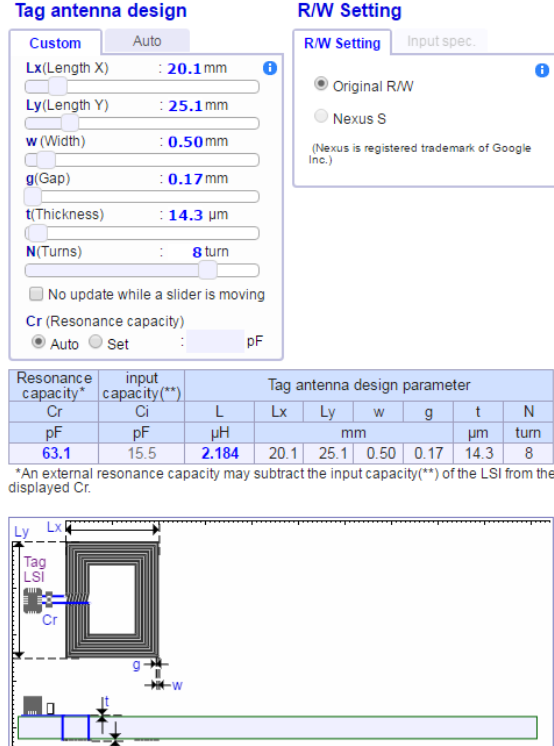


FIGURE 5.10: Panasonic NFC Antenna Online Tool. Taken from [8].

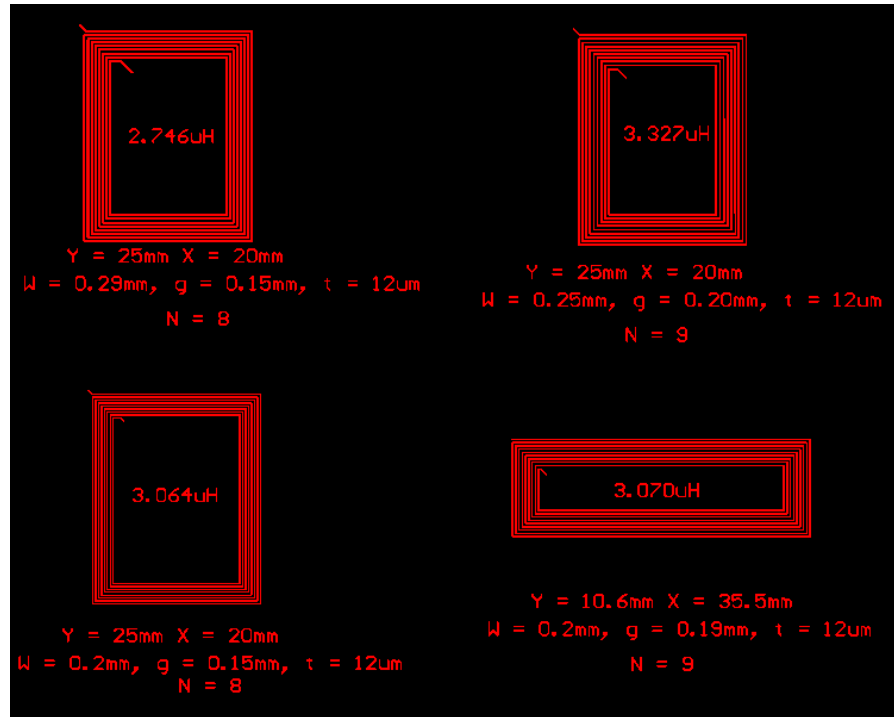


FIGURE 5.11: PCB Designed Antennas.

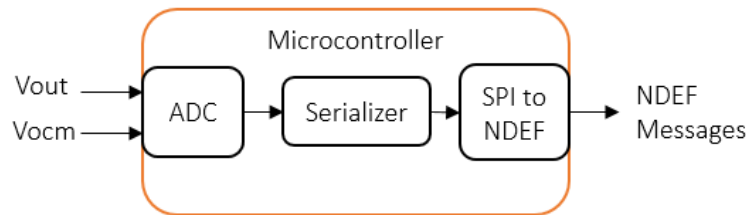


FIGURE 5.12: Microcontroller Module Requirements

5.3 Microcontroller

5.3.1 Requirements

The microcontroller serves the purpose of obtaining data from the read out circuit, while converting this data into a NDEF format to be sent to the smartphone. **Figure 5.12** describes the requirements for this module. The microcontroller would have to be capable of running at a low power, contains at least 2 ADCs for the LMP91200 data, and to be able to transmit via an Serial Parallel Interface(SPI) or I2C interface for the NDEF messages.

As there were a multitude of options, the decision was made to go with Atmel's ATTiny series, due to the availability of the software(Atmel Studio 7.0) on Imperial College servers as well as the programmer(Atmel-ICE) obtained beforehand for this project. However, there was still a range of options for the choice of microcontroller from the ATTiny range. Those that were viable for the project were compared and can be seen in **Table 5.2**.

5.3.2 Analysis of Options

The microcontrollers seen in the table contain at least 2 inputs pins for ADCs. However, they vary quite widely in terms of their data transmission schemes, as well as the number of I/O pins they have.

The power consumption was calculated based on the lowest possible clock frequency(128kHz) for the microcontroller at an expected VCC of 3.3V. This was done by observing the active power characteristics of the microcontrollers from their respective datasheets. Considering that data transmit speed is not a key criteria, the aim was to utilise the microcontroller at the lowest possible speed. This was added to the power consumption of their ADCs for an overall approximate power consumption of the microcontroller.

Microcontroller	Power (Active + ADCs)	I/O Pins	Data Transmission Scheme	Source
ATTiny10	0.33mW(128kHz)+1.452mW	4	bit-banging	[57]
ATTiny85	0.594mW(128kHz)+0.396mW	6	USI	[9]
ATTiny20	0.165mW(128kHz)+0.907mW	12	SPI	[58]
ATTiny102	0.165mW(128kHz)+0.825mW	6	USART	[59]

TABLE 5.2: ATTiny Microcontroller Options

The decision was made to use the ATTiny85 due to its small footprint, as well as the USI capability of being configured for both I2C and SPI interfaces. Given that the AS3955 chip comes with an SPI and I2C format, this would be useful for testing both interfaces if time permits. The power consumption of the IC was also at **0.99mW**, which was ideal for low power work.

5.4 Chapter Summary and Final Proposed Circuit

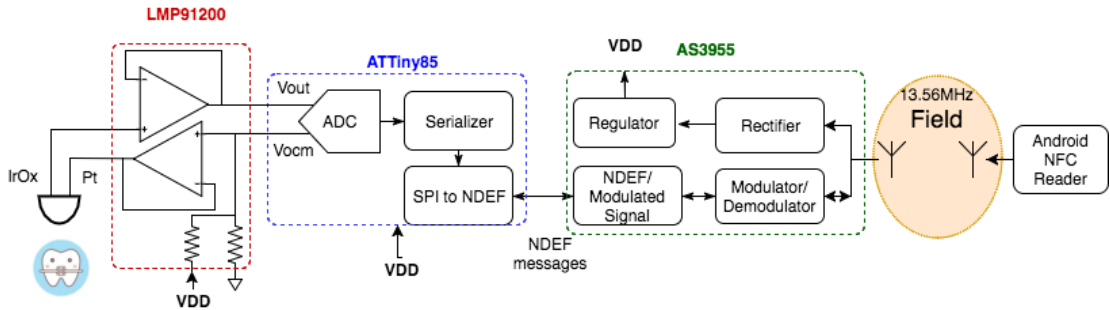


FIGURE 5.13: Block Diagram of Proposed pH-monitoring system

In this chapter, the NFC protocol is explained, with its key modules described. The antenna design process is shown, and the rationale behind the choice of the microcontroller is described.

Given that all the modules required in the SOB has been finalised, the overall system for the pH-monitoring system is proposed in **Figure 5.13**. All the modules described in **Chapters 3, 4 and 5** are integrated as shown.

The pH sensing is performed by the IrOx and Pt reference electrodes. In order to read the voltage values from the IrOx electrode, a way of holding the output voltage stable for a microcontroller's ADCs to read is required. Similarly, a stable reference voltage is required for the reference electrode in order for a stable comparison to the potential from the IrOx electrode.

This read out circuit required would involve two voltage buffers with negative feedback applied, to ensure that the reference electrode would obtain a stable voltage reference,

and the sensed voltage would have a stable output. This is done by the LMP91200 IC from TI, which was chosen for its low power($165\mu\text{W}$), as well as its internal potential divider that provided a reference voltage. This reduced the need for additional external resistors.

The output of the read out circuit is then fed into an ADC to obtain a value of the voltage. As the voltage output from VOUT-VOCM is linearly related to the pH of the solution, the pH value can be obtained. This pH value is transmitted via NFC Forum Data Format(NDEF) through an SPI interface to the NFC IC. The microcontroller used in this case is the ATTiny85, which is similarly chosen for its low power(0.99mW), as well as its ability to be configured for I²C and SPI interfaces.

The received messages are then converted into a modulated signal by the NFC Tag Logic available in the AS3955. This signal is then transmitted through the field via load modulation. This varies the resonant state between the resonant state between the reader and the tag, allowing the reader, in this case an Android smartphone, to obtain the data.

The AS3955 also contains a rectifier, which rectifies the AC voltage obtained from the antenna into a DC voltage. This is then regulated into a set regulated voltage for powering the remaining two components.

Chapter 6

Individual Module Tests

This chapter will focus on testing each of the modules beforehand to ensure that the power consumption for each of the components correspond to the theoretical expectations. The functionalities of each module were also tested to ensure that they would be able to work when integrated together.

This method reduces the complexity for debugging, and was useful in understanding each of the modules well before integrating them into a larger circuit.

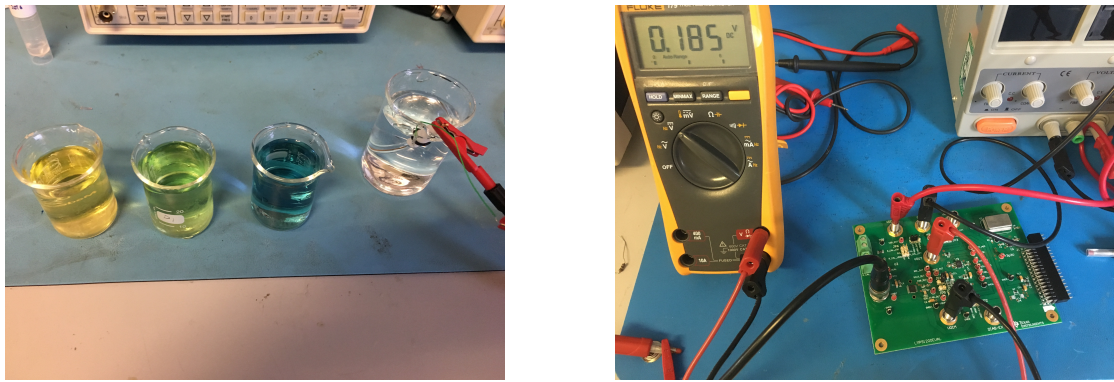
6.1 pH Tests

The pH sensing consisted of 3 main tests:

1. Testing the IrOx and reference electrodes with the read out circuit and observing for a linear relation between pH and voltage output.
2. Response time for sensors to output correct values.
3. The power consumption for the LMP91200 is as expected.

6.1.1 Experimental Setup

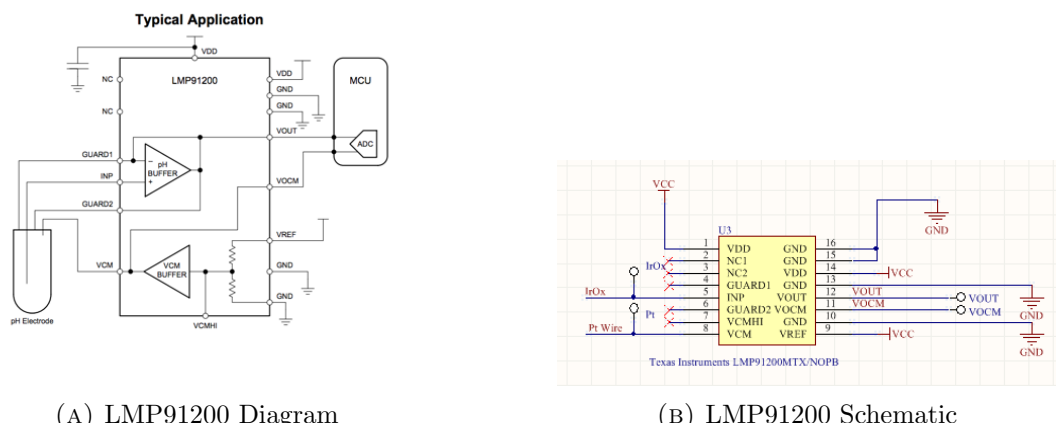
In order to test the electrodes, 3 solutions of varying pH of 5, 7 and 9 were set up. This was done by dissolving Hydrion Buffer[60] in distilled water. Coloring was added in order to further differentiate the three solutions, as seen in [Figure 6.1a](#). Lastly, a beaker of distilled water is used to clean the electrodes after each test.



(A) Prepared pH buffer solutions. pH 5(Yellow), pH 7(Green) and pH 9(Blue)

(B) LMP91200EVAL Board with set up

FIGURE 6.1: Circuit Setup for pH Tests



(A) LMP91200 Diagram

(B) LMP91200 Schematic

FIGURE 6.2: LMP91200 Configuration

Next, the IrOx electrodes, as well as the AgCl and Pt reference electrodes were set up for the experiment. An additional Iridium wire was prepared for use as a reference electrode. These were then connected to the LMP91200 IC through the use of an evaluation board. The output from the LMP91200 was then measured through the use of a multimeter as seen in **Figure 6.1b**.

Figure 6.2b describes the schematic setup for the LMP91200 IC. A 3.3V supply is used as the power supply(VDD) pin as well as the reference voltage(VREF) pin. As the LMP91200 contains an internal potential divider which divides the voltage by a factor of 2 as shown in **Figure 6.2a**, a 1.65V output is supplied at the VCM pin.

The VCM pin is then connected to the AgCl reference electrode, while INP pin is connected to the IrOx electrodes. The outputs at the VOCM and VOUT pins are measured using a multimeter.

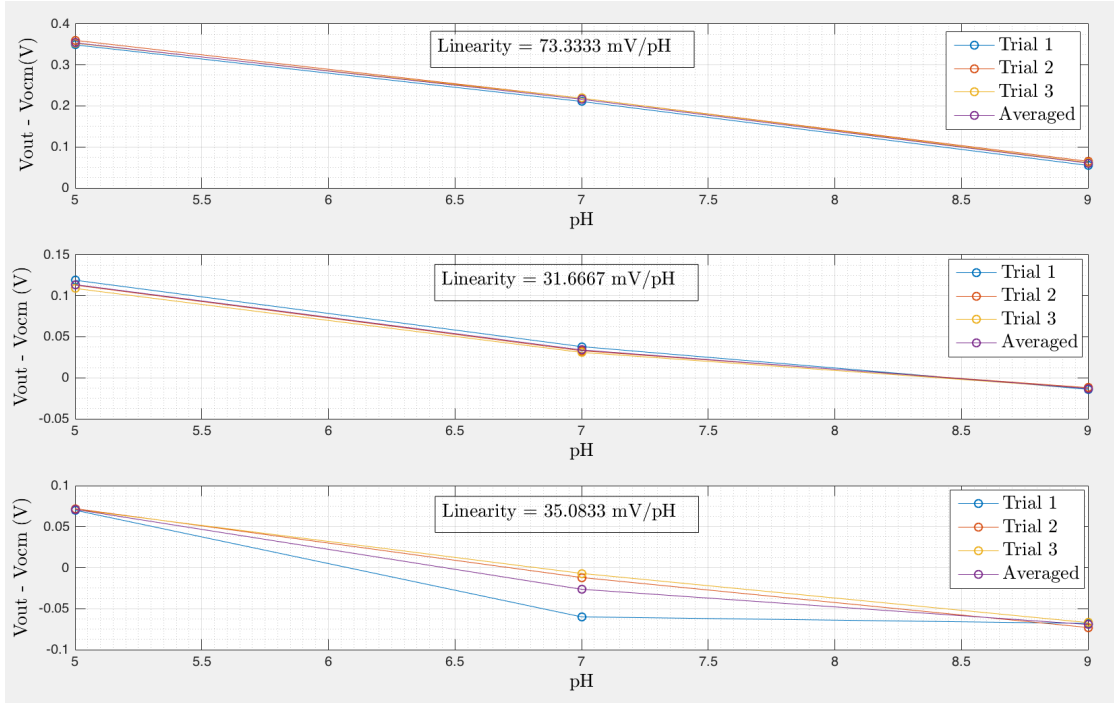


FIGURE 6.3: pH measurements acquired with fabricated IrOx electrode and three different reference electrodes: IrOx and AgCl on the top, IrOx and Ir Wire in the middle, IrOx and Pt Wire on the bottom. Linearity is stated in each figure.

6.1.2 Experiment 1: Linearity of Electrodes

The first round of tests measured the values of the IrOx electrodes and the AgCl reference electrodes to determine the sensitivity. The value of $V_{OUT}-V_{OCM}$ was measured for pH 5,7 and 9, before being repeated for 3 trials. These trials were then averaged, from which the obtained linearity was -73.33mV/pH .

However, as mentioned in **Section 3.3.3**, the AgCl reference electrodes are quite large, and a more ideal reference electrodes in terms of size would be the use of Pt cuffs. The above tests were repeated with the use of a Ir reference wire, and finally with a Pt wire as a reference.

The results can be seen in **Figure 6.3**. A common trend is observed, where the value of $V_{OUT}-V_{OCM}$ decreases as the pH increases. The sensitivity for the AgCl electrodes in tandem with the IrOx electrode demonstrate the highest sensitivity, at -73.3mV/pH . On the other hand, the sensitivity changes when the Pt reference electrodes are applied. This drops to around -35mV/pH , and -31mV/pH when Ir wires are used as a reference.

This may be due to the use of glass electrodes for the AgCl reference electrode. As glass electrodes have higher internal resistance[61], this results in less noise being applied to the reference voltage, as compared to the use of a Pt wire reference. In this case, a -35mV/pH value is still sufficient for our purposes.

On the other hand, the sensitivity between Pt and Ir reference electrodes are quite similar. However, as Pt shows slightly higher sensitivity, it is chosen as the reference electrode for the SOB.

6.1.3 Experiment 2: Response Time

During the experiments, it was observed that the sensors required a certain amount of time to stabilise to the exact voltage value. This was also an issue described in [18]. In order to determine this response time value, an experiment was conducted where the electrodes were placed in different buffers. The timings for the response time were recorded and averaged for an approximate reaction time of the IrO_x electrodes. This was found to be **approximately 10s**.

This would have consequences in the event that the pH level in a user's mouth changes suddenly, and the pH electrodes are unable to keep up with measurements. However, as the use of the SOB is to measure the stable pH values roughly an hour after a user has eaten, this would not cause any expected issues with the readings.

6.1.4 Experiment 3: Power Consumption of the LMP91200

To measure the power consumption of the LMP91200, a multimeter was connected in series with the LMP91200 to obtain the current drawn. **This was 55 μ A at a voltage of 3.3V**. Hence, the power consumption of the LMP91200 is **181.5 μ W**. This tallied closely with the expected power consumption of 165 μ W and the expected supply current of 50 μ A.

6.2 Microcontroller Tests

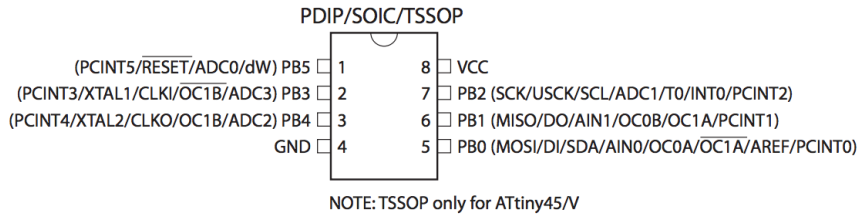


FIGURE 6.4: ATTiny 85 Pinout. Taken from [9].

There were 4 main functions to be tested for the microcontroller:

1. Slowing down the clock speed to 125kHz to reduce power consumption.
2. Ensuring the ADCs on the ATTiny85 are capable of measuring voltage values.
3. The Universal Serial Interface configuration as an SPI output for communication with the AS3955.
4. The power consumption of the ATTiny85 is as expected.

6.2.1 Experimental Setup

In order to test the ATTiny85, the IC was soldered onto a Small Integrated Outline Circuit(SOIC) to Dual-Inline Package(DIP) adaptor(**Figure 6.5a**) for testing on a breadboard as seen in **Figure 6.5c**. This was connected to an ATMEL ICE programmer obtained from CBIT. The software used to program the ATTiny85 is Atmel Studio 7.0.

The output of the microcontroller was observed with a logic analyzer from an Agilent Oscilloscope as shown in **Figure 6.5d**. This was useful for observing all the logic outputs from the microcontroller, in particular the SPI output signals as well as the clock timings. The last device that was used was a SPI decoder available on the Rohde and Schwarz HMO1002 oscilloscopes as shown in **Figure 6.5e**. This scope allowed debugging of SPI signals, and was useful for observing ADC values read from the microcontroller.

6.2.2 Experiment 1: ATTiny85 Clock Speed

There are 2 methods to change the clock speed of the ATTiny85. The first method involves changing the clock source of the ATTiny85. **Figure 6.6** displays the clock distribution diagram of the ATTiny85. The **Clock Multiplexer Module** allows a range of clock sources to be chosen. In order to choose the desired clock source, the microcontroller has to be set according to their flash fuses. These fuses are set by the software, and will remain the same even when power to the microcontroller is lost. The flash fuse bits can be seen in **Figure 6.7**, for which the internal 128kHz oscillator is the desired option.

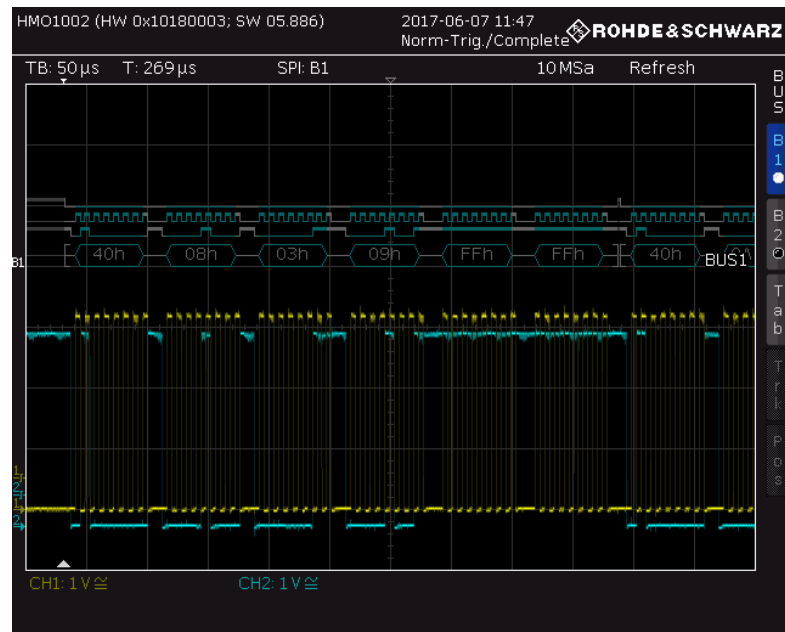
The other possible method used is to change the clock speed through a system clock prescaler. This prescaler applies a clock divider to the source clock, thus allowing the clock to be slowed down to a desired frequency. **Figure 6.8a** shows the register used for assigning the division factor, with bits CLKPS0 -CLKPS3 set according to the division factor. These bits can be set according to the table in **Figure 6.8b**.



(A) ATTiny85 on SOIC-DIP (B) ATMELE ICE Programmer (C) Breadboard Connections



(D) Logic Analyzer on Agilent Oscilloscope with SPI clock, MISO, MOSI and CS data



(E) SPI Decoder on Rohde and Schwarz Oscilloscope

FIGURE 6.5: Microcontroller Tests setup

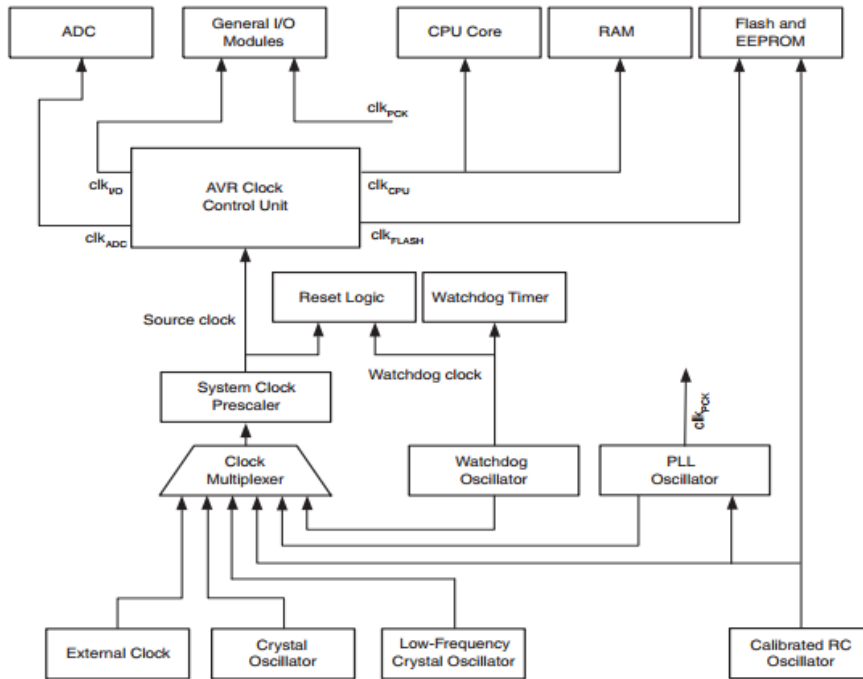


FIGURE 6.6: Clock Distribution Diagram of the ATTiny85. Taken from [9].

Device Clocking Option	CKSEL[3:0] ⁽¹⁾
External Clock (see page 26)	0000
High Frequency PLL Clock (see page 26)	0001
Calibrated Internal Oscillator (see page 27)	0010 ⁽²⁾
Calibrated Internal Oscillator (see page 27)	0011 ⁽³⁾
Internal 128 kHz Oscillator (see page 28)	0100
Low-Frequency Crystal Oscillator (see page 29)	0110
Crystal Oscillator / Ceramic Resonator (see page 29)	1000 – 1111
Reserved	0101, 0111

FIGURE 6.7: Close Source Selection. Taken from [9].

In order to write to the CLKPS bits, the CLKPCE bit has to be written to 1 with all other bits written to 0 for an enable. The rest of the bits can be written after this is done. This method was the chosen method due to it being easier to modify in code, and was implemented in the function `setclock` to lower the clock speed.

```
//Function for Varying Clock Speed
void setclock()
{
    CLKPR = 0x80; //To enable clock changes
    CLKPR = 0b00000011;//clock divide by 8 to 1Mhz(125kHz measured on clock
    //cycle)
}
```

CLKPR – Clock Prescale Register

Bit	7	6	5	4	3	2	1	0	
0x26	CLKPCE	-	-	-	CLKPS3	CLKPS2	CLKPS1	CLKPS0	CLKPR
Read/Write	R/W	R	R	R	R/W	R/W	R/W	R/W	
Initial Value	0	0	0	0	See Bit Description				

(A) Oscillation Calibration Register. Taken from [9].

CLKPS3	CLKPS2	CLKPS1	CLKPS0	Clock Division Factor
0	0	0	0	1
0	0	0	1	2
0	0	1	0	4
0	0	1	1	8
0	1	0	0	16
0	1	0	1	32
0	1	1	0	64
0	1	1	1	128
1	0	0	0	256
1	0	0	1	Reserved
1	0	1	0	Reserved
1	0	1	1	Reserved
1	1	0	0	Reserved
1	1	0	1	Reserved
1	1	1	0	Reserved
1	1	1	1	Reserved

(B) Table of Values for division factors

FIGURE 6.8: Clock Prescaler Select. Taken from [9].

The output clock speed was verified using the logic analyzer, and the frequency was measured as 125kHz as expected.

6.2.3 Experiment 2: Analog to Digital Converters(ADCs)

The ATTiny85 contain successive approximation ADCs that can be configured for single-ended or differential inputs. The reference voltage applied for the ADCs can be obtained from 3 sources: The VCC value on the power supply, an internal 1.1V reference or an internal 2.56V reference. A gain factor of x20 could also be applied on differential inputs in order to improve the resolution.

Hence, there are a number of things that need to be configured for using the ADCs:

1. Enabling the ADCs for the correct ports
2. Enabling single-ended or differential inputs
3. Setting the ADC clock prescaler
4. Determining the reference voltage source

MUX[3:0]	Single Ended Input	Positive Differential Input	Negative Differential Input	Gain
0000	ADC0 (PB5)	N/A	N/A	N/A
0001	ADC1 (PB2)			
0010	ADC2 (PB4)			
0011	ADC3 (PB3)			
0100	N/A	ADC2 (PB4)	ADC2 (PB4)	1x
0101 ⁽¹⁾		ADC2 (PB4)	ADC2 (PB4)	20x
0110		ADC2 (PB4)	ADC3 (PB3)	1x
0111		ADC2 (PB4)	ADC3 (PB3)	20x
1000		ADC0 (PB5)	ADC0 (PB5)	1x
1001		ADC0 (PB5)	ADC0 (PB5)	20x
1010		ADC0 (PB5)	ADC1 (PB2)	1x
1011		ADC0 (PB5)	ADC1 (PB2)	20x
1100 ⁽²⁾	V _{BG}	N/A	N/A	N/A
1101	GND			
1110	N/A			
1111 ⁽³⁾	ADC4			

FIGURE 6.9: ATTiny 85 ADCs Configuration. Taken from [9].

6.2.3.1 Single and Differential Inputs

The ATTiny85 contains 4 possible ADC ports(ADC0 - ADC3) as seen in [Figure 6.4](#). Each of these ports is capable of single-ended inputs. However, not all the ports are capable of differential inputs. As shown in [Figure 6.9](#), only configurations whereby ADC2/ADC3 and ADC0/ADC1 allow differential inputs. This was a mistake made in the Experimental PCB design, and rectified in the final prototyped design.

The equations for calculating the output voltage from the ADC values are shown below. The output from the single ended converter is given by the following [Equation 6.1](#):

$$ADC_{single} = \frac{V_{IN} \times 1024}{V_{REF}} \quad (6.1)$$

while the output from a differential input converter is given by [Equation 6.2](#):

$$ADC_{differential} = \frac{(V_{POS} - V_{NEG}) \times 512}{V_{REF}} \quad (6.2)$$

The advantage of having a differential inputs would be not having to calculate the value of VOUT-VOCM in software, as it would be done in hardware. Hence, differential input ports ADC2 and ADC3 were chosen for the final design in order to calculate VOUT-VOCM.

6.2.3.2 ADC Clock Prescaler

The ADC clock is recommended to run at a frequency of 50kHz - 200kHz for maximum resolution. In order to set this frequency, a clock prescaler, similar to the oscillator clock prescaler described previously for the ATTiny85, is set. This clock prescaler divides the system clock by a division factor for an appropriate ADC clock frequency.

This was set to **125kHz**, which was equal to the system clock. Testing the ADCs at this frequency yielded accurate readings.

6.2.3.3 ADC Voltage Reference

The reference voltage source was chosen to be the internal 2.56V. As VCC was supplied from the NFC field, the voltage fluctuations caused by changing orientations would affect the ADC values. Thus, having a stable voltage supply would be more conducive for the calculations.

On the other hand, the expected value to be read at the ADC inputs would be $1.65V \pm 100mV$. Thus, a reference voltage of 1.1V would be too low, and an overflow would occur.

All these configurations were set up as shown in the code snippet below. This was tested by applying a voltage to the ADC inputs, and observing the ADC outputs by sending them via SPI to the logic analyzer. The ADC outputs corresponded to **Equation 6.1** and **6.2**. The ADC software was implemented in `ADC2_ADC3` for the final prototype, and in `VOUT_VOCM` for testing with the experimental PCB. These functions can be seen in **Appendix A1**. Two functions are written as the ADCs used in the experimental PCB and final PCB are different.

6.2.4 Experiment 3: Universal Serial Interface(USI)

The ATTiny85 contained a unique serial interface called USI. This interface allowed for Serial Parallel Interface(SPI) as well as I2C communications to be configured from the same output bus. The code for the USI in SPI configuration can be seen in the function `SPI_write` from **Appendix A1**.

The ATTiny85 was configured as the SPI master, with the AS3955 the slave. There did not exist a specific SPI library, and hence the code in `SPI_write` involved writes to registers. Each of the writes had a specific function: To configure as SPI, to toggle the clock or to shift data.

Additionally, it is important to note that the USI contains specific ports for data outputs and data inputs(DO and DI). These ports should not be confused with the MISO and MOSI ports on the pin layout as seen in [Figure 6.4](#). This was a mistake that was made in the initial design of the PCB.

The USI output was tested using the logic analyzer. The output was found to be working appropriately, and was debugged using an SPI decoder.

6.2.5 Experiment 4: Power Consumption of the ATTiny85

After configuration of the ADCs and the SPI outputs, the power consumption of the ATTiny85 was measured. This was found to be **0.9mA at a 3.3V supply**. Thus, the power consumption for the ATTiny85 is calculated to be **2.97mW**. This is larger than the expected 0.99mW theoretical power consumption, which may be due to certain peripherals still running during code runtime.

6.3 NFC Tests

The NFC tests consisted of tests for 5 tasks:

1. Communication with the smartphone reader from the AS3955.
2. The AS3955 reader orientations and distances.
3. Varying the AS3955 output power supply.
4. Varying the antennas used for the AS3955.
5. The possible power output of the AS3955.

6.3.1 Experimental Setup

In order to test the AS3955 IC, the AS3955 demokit as seen in [Figure 6.10](#) was used together with a Google Nexus 5 smartphone with NFC capabilities. The demokit consisted of 3 tags, with an evaluation board that allowed for programming the voltages required using a software. In addition to this, an app was included that could be installed on an Android smartphone. The tags consisted of 3 different sizes: 20x25mm, 22x38mm, and 32x45mm. Each of these tags could be connected to the evaluation board through a ribbon cable for configuration.



FIGURE 6.10: AS3955 Evaluation Board with NFC Tags

6.3.2 Experiment 1: NFC Communication with the smartphone from the AS3955

The first experiment involved being able to read the the tags using the Google Nexus 5 smartphone. To do this, the NFC settings were enabled on the smartphone as seen in **Figure 6.11a**. The AS3955 software was also installed on the smartphone as shown in **Figure 6.11b**. This software allows for monitoring the data values on the AS3955 tags.

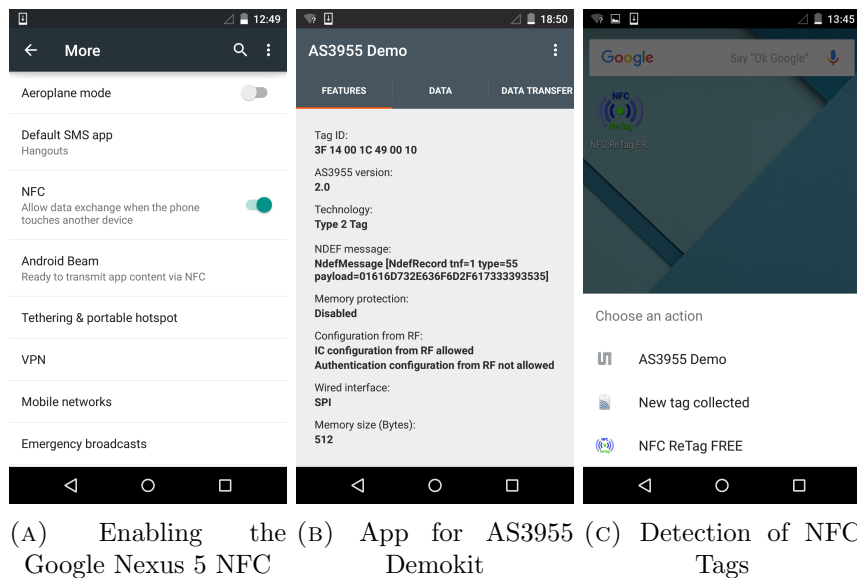


FIGURE 6.11: Android Software Configuration

The software was tested with the tags provided. This was done by placing the tags on the rear of the smartphone near the NFC antenna location. On detection, a "bleep" sound is given out by the smartphone, and a screen displays that the NFC tag has been detected as seen in **Figure 6.11c**. On opening the AS3955 demo application, it is possible to observe the data stored in the AS3955 EEPROM.

6.3.3 Experiment 2: AS3955 Reader Orientation and Distances

The AS3955 and Nexus 5 reader orientation and distance was tested to obtain a value for the threshold distance for operation. The threshold distance is the minimum distance whereby the AS3955 IC would obtain enough power to begin powering up, and in the process begin supplying a voltage output. **Figure 6.12** describes the setup for this experiment.

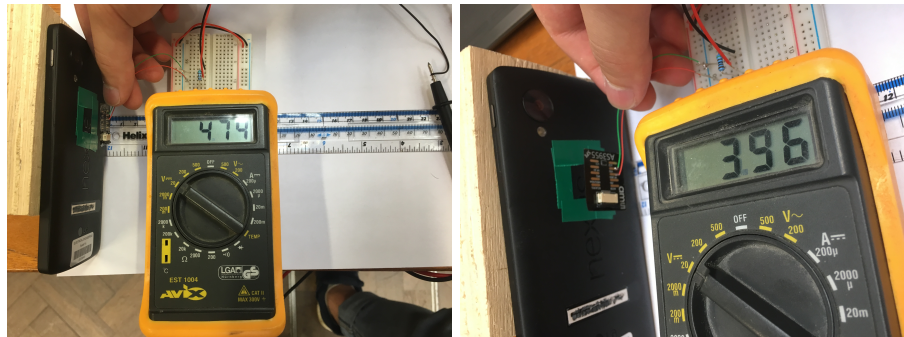


FIGURE 6.12: Tag Operation Distance

The Nexus 5 was placed on a wooden block, while the tag distance from the reader was varied accordingly. The green square on the Nexus 5 indicates the optimum point for NFC sensing, which was verified through experimentation. A multimeter was used to measure the voltage output from the tag as an indicator of the AS3955 powering up.

The threshold distances for the AS3955 operation varied according to the tag sizes as shown in **Table 6.1**. This is as expected, with a larger coil being able to capture more of the field as possible. However, the threshold distances did not vary by much, with the smallest tag operating at a distance of 35mm, while the largest tag operation distance was at 42mm.

Tag Size(mm)	Threshold Distance(mm)
20x25	35
22x38	39
32x45	42

TABLE 6.1: Threshold Distance of Operation for AS3955 Tags

It is also important to note the orientation of the tag as seen in **Figure 6.12**. The tag coil has to be placed parallel to the back of the Nexus 5, with any slight angular variation causing the threshold distance to drop.

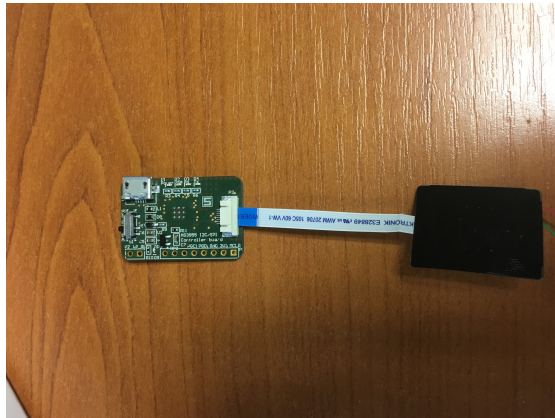


FIGURE 6.13: Connecting the Tag to the Evaluation board

6.3.4 Experiment 3: Varying the output power supply from the AS3955

As mentioned in [Section 4.6](#), it is possible to vary the output voltage from the AS3955. However, although the AS3955 Smartphone app on the Nexus 5 allows reading and writing the data, it does not allow configuration of the output voltage. In order to configure this, the AS3955 demo software on the PC was used.

[Figure 6.13](#) displays the evaluation board connected to the tag. This evaluation board can then be connected to a PC through a mini-USB cable for use with the AS3955 software. This software allows for configuration of the output voltage as well as the output impedance of the supply. The software was tested, and was found to be working accurately.

6.3.5 Experiment 4: Varying the Antennas used on the AS3955

To determine whether it was possible to utilise commercial antennas with the AS3955, one of the tags was modified for use with external antennas. This was done by cutting the antenna tracks from the pads, and soldering wires to the pads to be connected to external antennas as seen in [Figure 6.14](#).

In order to connect the antennas to the AS3955, capacitive compensation is required to ensure that the resonance of the LC tank is kept at 13.56MHz as mentioned in [Section 5.2.2.1](#). This was done for all the antennas.

During the tests, it was found that none of the commercially applied antennas could work. This was probably due to the requirement for an impedance matching circuit, or due to the size of the antenna being too small to obtain the required power for the AS3955 to start up.

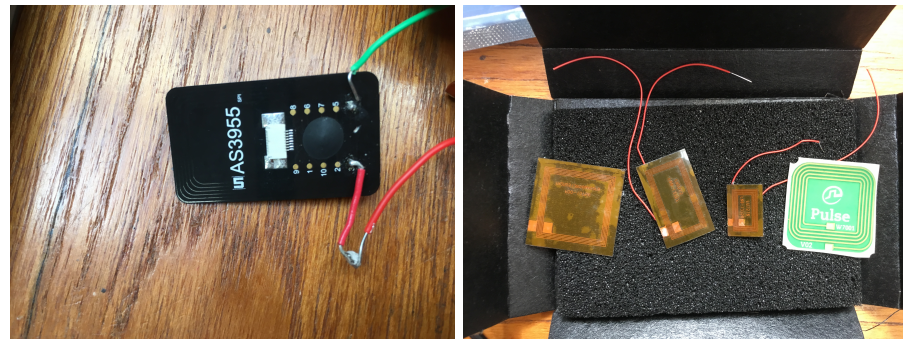


FIGURE 6.14: External Antenna for NFC Tag

In lieu of this, the antenna was designed from scratch using a PCB based on the working 20x25mm NFC tag design. This will then be implemented on an experimental PCB.

6.3.6 Experiment 5: Output Power supplied by the AS3955

The 20x25mm NFC tag was tested for its output power after being regulated to 3.3V. The distance between the tag and the reader was kept constant at 10mm, while the voltage across the output supply of the NFC tag was dropped across varying loads as shown in **Table 6.2**.

Load Value(Ω)	Voltage Measured(V)
0	4.76
50	0.17
100	0.34
500	1.56
1k	3.3
2k	3.3
5k	3.3
10k	3.3

TABLE 6.2: Output Voltage across Varying Load Values at a constant distance of 10mm

At very low load values(50 - 500 Ω), the current drawn by the load is too high, as per the $I = \frac{V}{R}$ relation. This causes the output voltage to drop below the regulated 3.3V.

At $1\text{k}\Omega$, the output voltage value begins to stabilise at 3.3V. Hence, this load value is used to calculate the power supplied using the $P = \frac{V^2}{R}$ relation. This gives around **10.9mW** of power. This is less than the theoretical maximum of 5mA at 4.8V which

should provide 24mW of power, and is probably due to the size of the 20x25mm tag as compared to the larger tags. However, this power is sufficient for the remainder of the components.

6.4 Chapter Summary

The individual module tests allowed for verification of the power required for the components, as well as an individual check for the functionalities of the modules. The power supplied(10.9mW) would be sufficient for both the ATTiny85(2.97mW) as well as the LMP91200($181.5\mu W$). However, this is based on the design of the 20x25mm AS3955 demo tags. As commercial options did not work, it is imperative to examine whether designed PCB antennas were capable of supplying the same power output. This is done in the following chapter.

Chapter 7

Overall Module Tests

This chapter would focus on the communications between each of the modules, as well as the power supply for the entire board. This would involve: decoding of the ADC read voltages into pH values, converting the SPI output into the NDEF format for data transfer, and lastly designing the antenna on a PCB. These tests would be done on a breadboard as well as through a printed circuit board(PCB).

7.1 Breadboard Tests

The experiments to be conducted are the following:

1. Check that ADC inputs from the LMP91200 work as expected.
2. Communications from the LMP91200 to ATTiny85.
3. Communications from the ATTiny85 to AS3955.
4. Full system characterisation, from pH read at electrodes to AS3955 EEPROM.

7.1.1 Experimental Setup

A breadboard was used to connect all the modules together according to the schematic in [Figure 7.1](#). The ATTiny85 and LMP91200 was soldered onto a SOIC-DIP adaptor, while wires were soldered to the AS3955 NFC tag pins for connection to the breadboard. The components were then wired together for tests, with the AS3955 20x25mm NFC tag supplying power to the entire breadboard as seen in [Figure 7.2](#).

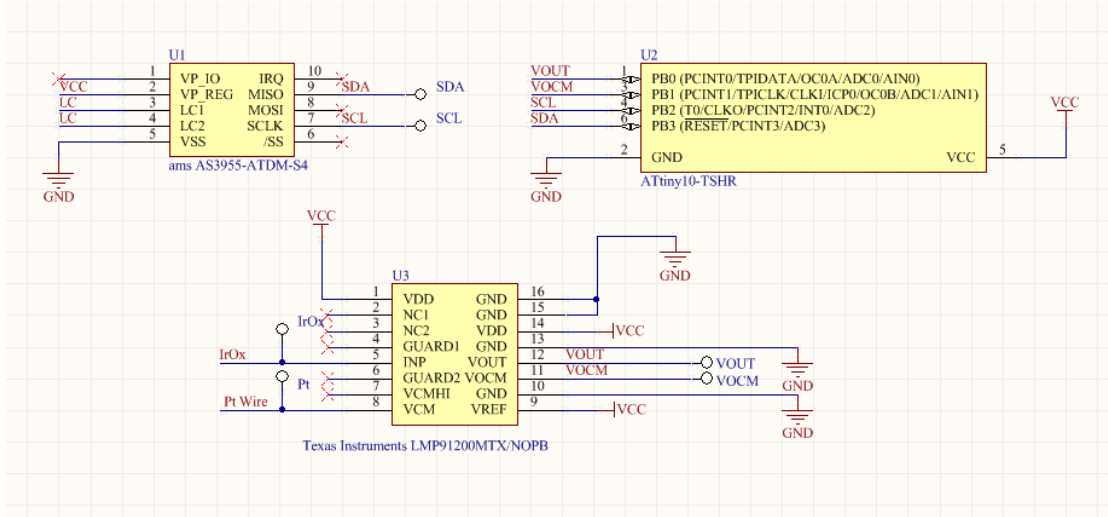


FIGURE 7.1: SOB Schematic

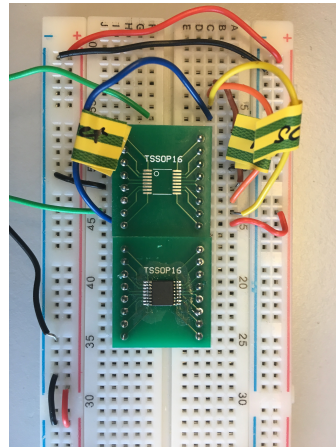


FIGURE 7.2: Breadboard Testing

7.1.2 Experiment 1: Electrodes to LMP91200

The IrOx and Pt electrodes were connected to the INP and VCM pins on the LMP91200. As the board was powered up by the AS3955, it was observed that the voltage output from the AS3955 tended to fluctuate slightly around the range of 3.3V.

This may be an issue in regard to the reference Pt electrode, which is the value of $VCM = VDD/2$. Thus, a fluctuating supply would cause a change in the reference voltage as well as a change in the calibrated readings. However, it is also noted that the reference voltage does not change rapidly. That meant that it took a while for the reference voltage to rise to the expected voltage value of $VDD/2$, and also did not change rapidly when the VDD fluctuated. This characteristic was useful in the application of the reference voltage.

7.1.3 Experiment 2: LMP91200 to ATTiny85

The communications from the LMP91200 would involve two implementations. First, to determine the accuracy of the ADCs, and second, to convert the ADC values to an approximate pH value to be sent.

7.1.3.1 ADC Accuracy

To test the accuracy of the ADCs, the readings from the ADC were sent via SPI to the SPI decoder for viewing. For a reference voltage of 2.56V, the supply voltage has to stay above 3.0V. Even though the reference voltage as measured from VO_{CM} fluctuated slightly according to the supply, the ADC's reference voltage stayed constant at 2.56V. Thus, the readings remained accurate throughout fluctuating voltage values.

7.1.3.2 ADC Decoder

To decode the ADC values to the pH value, the linear relation between V_{OUT}-VO_{CM} and the pH values was used. Recalling the tests in [Section 6.1.2](#), it was observed that the linear relation between the pH values and the V_{OUT}-VO_{CM} is as shown in [Equation 7.1](#).

$$V_{OUT} - V_{OCM} = (-35mV/pH)pH + 0.750mV \quad (7.1)$$

Hence, we can manipulate this equation to form [Equation 7.2](#):

$$pH = \frac{(V_{OUT} - V_{OCM}) - 0.750mV}{(-35mV/pH)} \quad (7.2)$$

Thus, the value of the pH could be obtained from three values: the linearity of the electrodes, the offset voltage at pH 5, and the value of V_{OUT}-VO_{CM}. This is shown in the function `decode_ADC` in the [Appendix A1](#).

7.1.4 Experiment 3: ATTiny85 to AS3955

To test that the data sent through SPI were working, NDEF messages were sent to the EEPROM of the AS3955 to be written into the memory. This data was then read from the NFC tag from the smartphone.

The format for sending NDEF messages is explained previously in [Section 5.1.1](#). To implement this, a function was written for writing to the EEPROM block in the AS3955. This is described in the function `write_NDEF` in the [Appendix A1](#).

Data sent to the AS3955 was observed from the smartphone data. Thus, the entire system was capable of working as a single unit.

7.1.5 Experiment 4: Full System Characterisation

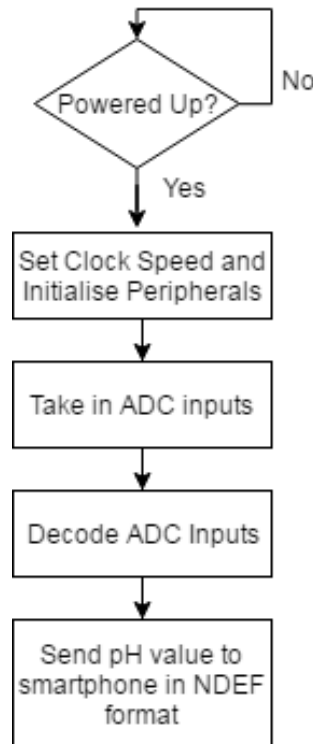


FIGURE 7.3: Flow diagram of software

The final test was to perform a full system characterisation. This would entail the Nexus 5 powering up the entire circuit, and the LMP91200, ATTiny85 and AS3955 performing their required functions. [Figure 7.3](#) describes the software implemented in the ATTiny85 for the throughput tests.

On powering up, the microcontroller would begin initialising the required peripherals. Next, the values from the ADCs would be taken, and decoded into a pH value. This pH value is then sent to the smartphone. This is implemented in the function `main` in [Appendix A1](#). Testing this revealed that the pH could be read from the ADCs. Some issues remain as explained above in regards to the fluctuating power supply that is dependent on the orientation of the tag to the smartphone. However, the overall system is able to communicate accurately, which was the aim of the breadboard tests.

7.2 Experimental PCB

With the overall board tests a success, the next stage was to design specific antennas on PCBs. The first PCB that was designed was an experimental PCB, with multiple antennas designed that could be interchanged with the AS3955.

7.2.1 Design of Experimental PCB

The main aim of the experimental PCB was to **test the design of NFC antennas**. As the commercial antennas tested in the individual module were unable to interface with the AS3955, it was important to experiment with the design of multiple antennas during this step.

7.2.1.1 Requirements

The requirements for the experimental PCB can be summarised as the following:

1. Ease of testing for each of the individual components.
2. Testing different types of NFC antennas designed.
3. Header for programming the microcontroller.
4. External connection to NFC tag for contingency in the case that PCB antenna fails to interface.
5. Testing if a ground plane below an antenna affects its properties.

7.2.2 PCB Design

The PCB schematic can be seen in [Figure 7.4](#), while [Figure 7.5](#) and [Figure 7.6](#) shows the PCB layout and its 3D version respectively.

7.2.2.1 Electrode Pad Points

The electrode pad points for the IrOx and Pt sensors allow for a compact version of the electrodes to be soldered on. These pad sizes were determined based on the size of the planned prototype, and was implemented for testing on pH solutions.

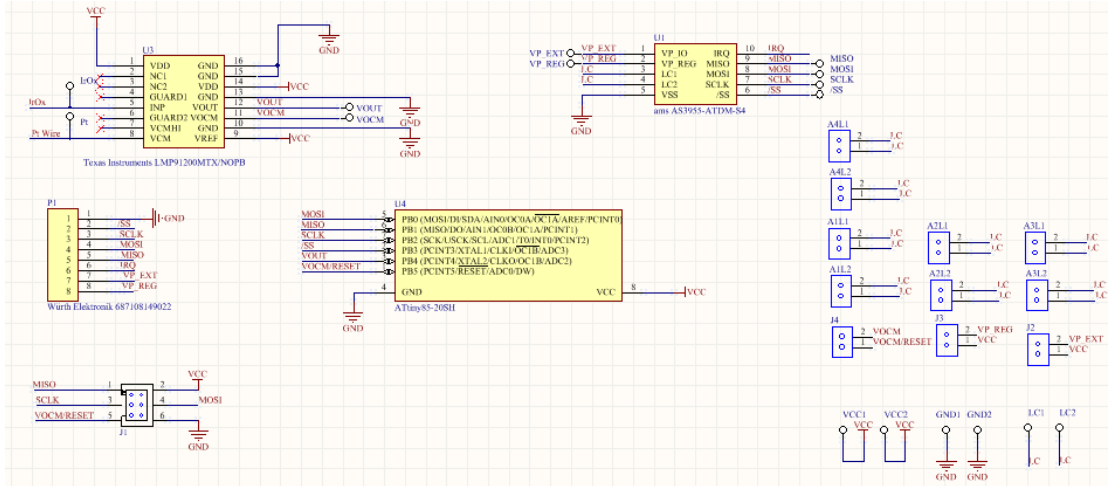


FIGURE 7.4: PCB Schematic

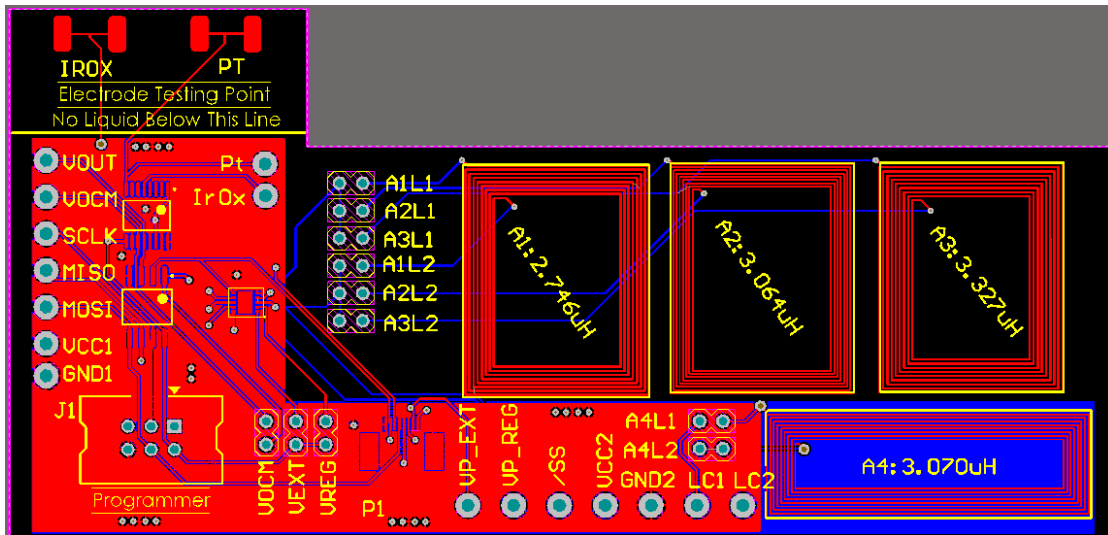


FIGURE 7.5: PCB Layout

7.2.2.2 Testpoints and Headers

Multiple testpoints were added for the pins along the edges for ease of prototyping. In addition to this, a header was added for the ATMEL ICE programmer in order to allow easier programming of the ATTiny85. P1 also displays the female header for the ribbon cable for connection with an external NFC tag antenna, or for use with the AS3955 evaluation board.

7.2.2.3 Antennas

A1 - A4 represent 4 different antennas as designed previously in **Section 5.2.2.2**. A2 represents the optimum antenna inductance at around $3.064\mu\text{H}$, with A3 being at around

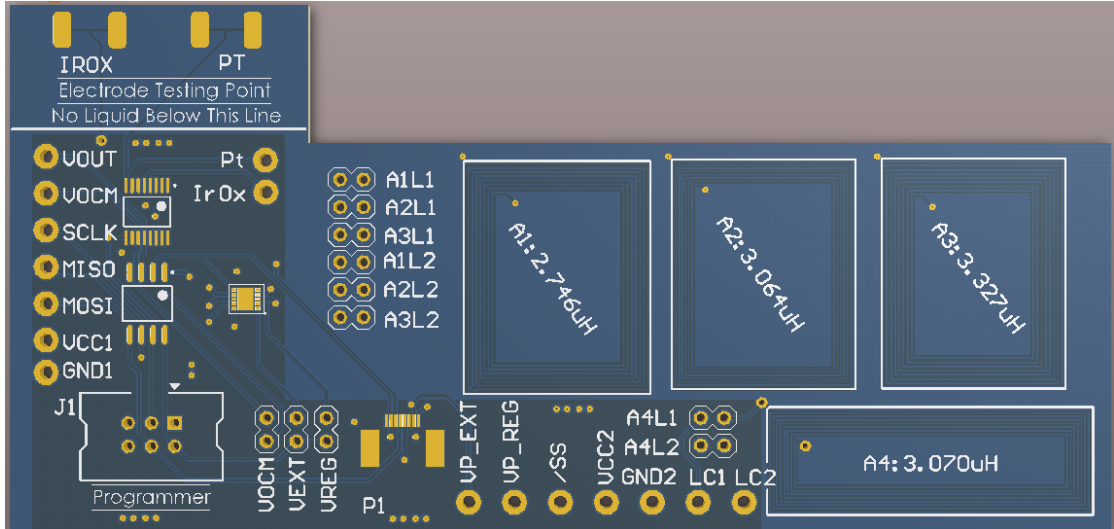


FIGURE 7.6: PCB 3D View

110% of that value, and A1 being at 90% of that value. This was as the PCB manufacturer would alter the inductance value slightly, and thus these three antennas would be tested for the optimum power. A4 represents an antenna with a ground plane below, to determine whether a ground plane added in the final prototype would affect the antenna properties.

A1L1 to A4L2 correspond to the different antennas that could be swapped for use with the AS3955. These antennas could be swapped through headers placed on the pin.

7.2.2.4 PCB Substrate

Lastly, the PCB was fabricated on a FR-4 substrate, at 1mm thickness for the board and $12\mu\text{m}/\frac{1}{2}\text{oz}$ thickness for the copper layer. The copper thickness was chosen based on the estimated calculations of the inductance of the antennas.

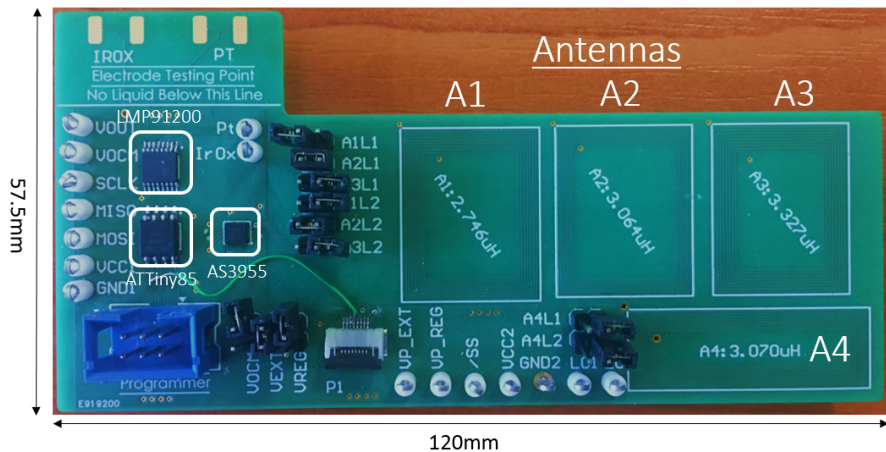


FIGURE 7.7: Fabricated PCB with components annotated.

Figure 7.7 shows the final PCB with all the components soldered on. The components are annotated together with the antennas.

7.2.3 Experiment 1: Testing NFC Antennas

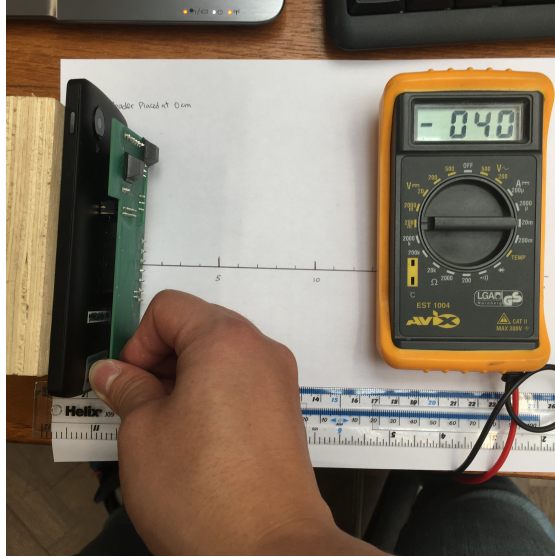


FIGURE 7.8: Antenna Tests

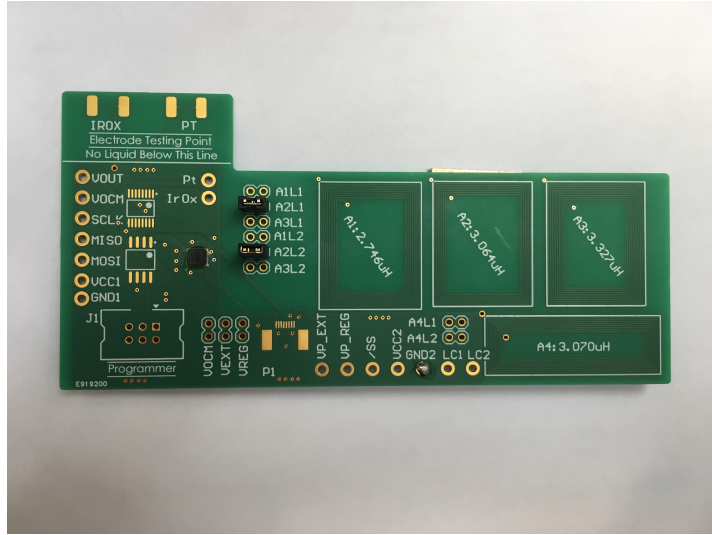
This test involved checking if the antennas could interface with the AS3955. Antennas A1, A2 and A3 were capable of doing so, while antenna A4, with a base ground plane, was unable to achieve communications. Thus, further tests were done on ground planes in **Section 7.2.4**.

Figure 7.8 describes the experiment conducted for determining the threshold operation distance for each of the three working antennas, where the minimum power could be supplied. The results are shown in **Table 7.1**.

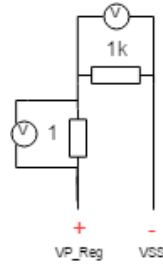
Antenna No.	Simulated (μH)	Measured (μH)	Max distance (mm)	Power Drawn from Antenna (mW)
A1	2.746	2.8	31	4.2
A2	3.064	3.1	35	6.3
A3	3.327	3.3	32	4.6

TABLE 7.1: Antenna Characterization results

The results show that A2 is the best performing antenna, with A1 and A3 having slightly shorter threshold distances before it can interface. This corresponds with the optimal inductance value, and indicates that A2 would be the best design moving forward in the final prototype.



(A) PCB with only AS3955 component for power supply measurements



(B) Schematic for power supply calculation

FIGURE 7.9: Antenna Power Supply Tests

To test the power supply of the antennas, the AS3955 was soldered onto the PCB without any other components attached as shown in [Figure 7.9a](#). To measure the power, the voltage of the output of the AS3955 regulator was measured across a $1\text{k}\Omega$ load as shown in [Figure 7.9b](#). The current output was measured by connecting a 1Ω resistor in series with the device. The voltage measured across this 1Ω provided an indication of the current. These two values were multiplied together for the power. The power output from each of the antennas was measured as shown in [Table 7.1](#).

The results show that the power output from the AS3955 demo tag is higher, which may possibly be due to a different substrate used. Another possibility could be that the inductance of the fabricated antenna was not exactly at $3.061\mu\text{H}$, which is required. This could be explored in the future work.

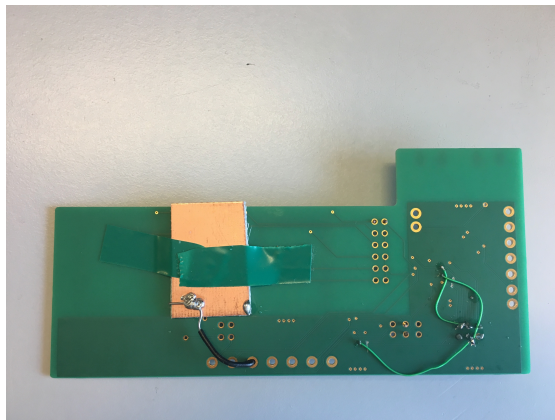


FIGURE 7.10: PCB Ground Plane Tests

7.2.4 Experiment 2: Ground Plane on Antenna

As mentioned previously, antenna A4 was unable to work with the AS3955. To further verify if a ground plane was the source of the issue, a copper plate was stuck behind antenna A2 as shown in [Figure 7.10](#).

The Nexus 5 was then applied to the field to interface with the AS3955. However, all attempts at interfacing failed. In order to understand this effect, research was done into the possible impact of metal near antennas.

A paper on the effect of metal plates near folded dipole antennas[\[62\]](#) corresponds with this occurrence. In their experiments, it was discovered that the presence of a metal plate at the right distance near an antenna would cause changes to its resonant frequency and impedance. Hence, it can be assumed that the presence of the metal plate would cause the resonant frequency of the antenna A2 to vary, resulting in the inability to draw power from the 13.56MHz field from the Nexus 5.

This resulted in the design of the final prototype avoiding the use of a base ground plane to avoid any interference with the resonant frequency of the antenna.

7.2.5 Experiment 3: Throughput Tests

The last tests involve tests on the entire system. Similarly, the pH solutions were prepared, and the board was used to test the system as shown in [Figure 7.11](#).

The readings taken using the experimental PCB is shown in [Table 7.2](#). As can be seen, there was a slight offset observed from the readings taken the first time. This was probably due to a slight offset from the linear relation, which was corrected by varying the parameters in the function `decode_ADC` as per [Equation 7.3](#).

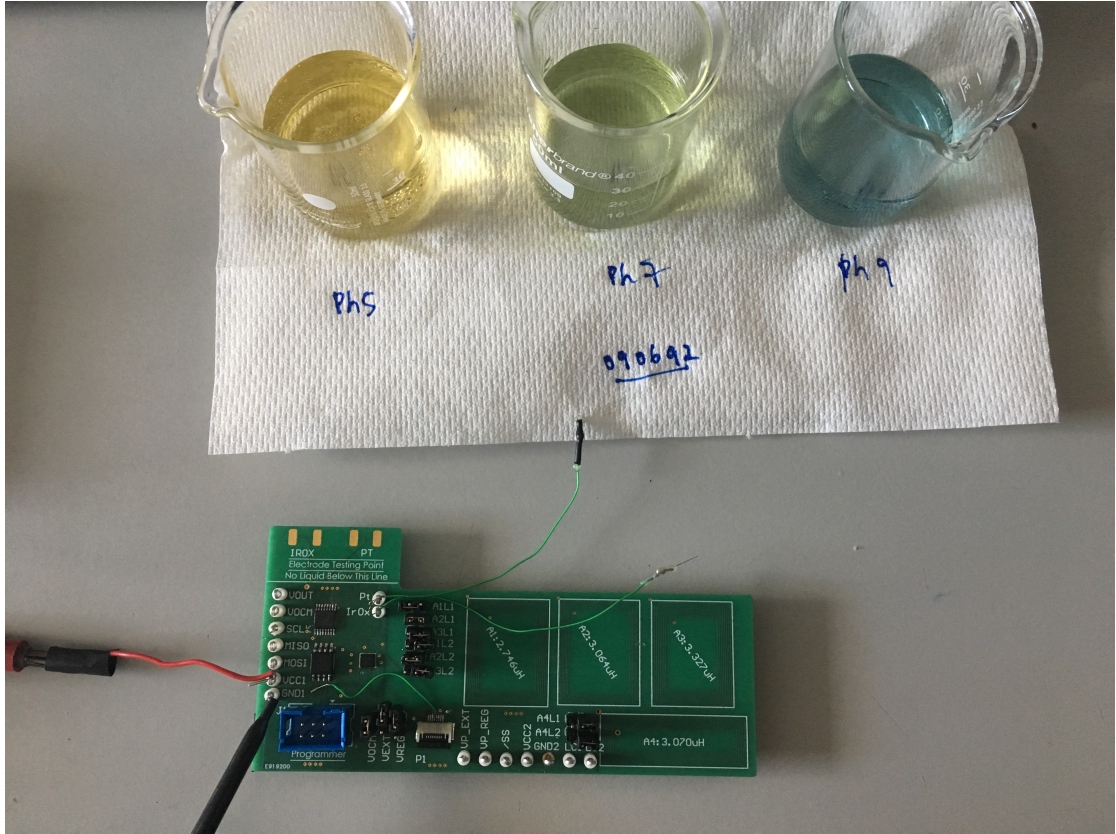


FIGURE 7.11: Throughput Tests with Experimental PCB

Readings			
pH Solution	SOB Measurement 1	SOB Measurement 2	
5	5.1	5.0	
7	7.2	7.0	
9	9.2	9.0	

TABLE 7.2: pH tests with implemented PCB

$$pH = \frac{(V_{OUT} - V_{OCM}) - OFFSET}{(-LINEARITY mV/pH)} \quad (7.3)$$

This was calibrated, and the next measurements showed that the readings were exactly at pH 5, pH 7 and pH 9.

Hence, throughput tests were capable of reading a pH value from the solution applied at the electrodes. This was read directly from the Nexus 5 smartphone. However, there remained issues in regards to the sensitivity of the electrodes, as well as the power supply.

The electrodes sensitivity was observed to degrade over time. Hence, the calibrated linearity of the electrodes would vary, thus causing the approximated pH readings to be inaccurate. The resulting change in the linearity would have to be modified internally in the microcontroller software to ensure accurate pH readings. Hence, future work could

look to find a way to automatically calibrate the microcontroller by having a function that calculates the parameters when the SOB is placed in a stock solution.

The power supply of the AS3955 would vary with the distance of the smartphone from the antenna. This is solved by changing the output resistance of the AS3955 supply, as well as varying the supply voltage to be higher than the expected 3.3V.

7.3 Chapter Summary

This chapter shows that the antennas designed on the PCB are capable of powering the LMP91200 as well as the ATTiny85. Communication between each of the modules are also verified. This allows the final prototype to proceed with the working antenna, as well as the encapsulation of the final device.

Chapter 8

Final Prototype and Evaluation

After the tests on the modules, integrating them, and designing a working antenna capable of powering the entire system, it was decided to put together the final prototype for the SOB. This would then be evaluated to determine if the specifications determined beforehand are met.

8.1 Final Prototyped Device



FIGURE 8.1: Envisioned SOB Fitting on retainers, with SOB covered with epoxy. The SOB is placed on the outer layer of the retainers to avoid interference with user's jaw motion.

The requirements for the final prototyped SOB are similar to the specifications given at the start:

1. To be able to read pH values from 5-8.
2. To be small enough to be placed in the mouth.
3. To be powered wireless and transmits data wirelessly.
4. Biocompatible encapsulation.

Considering that all these requirements can be met using the components sourced beforehand, the final prototype is designed based on all the previous experiments with the fitting similar to that in **Figure 8.1**.

8.1.1 PCB Design

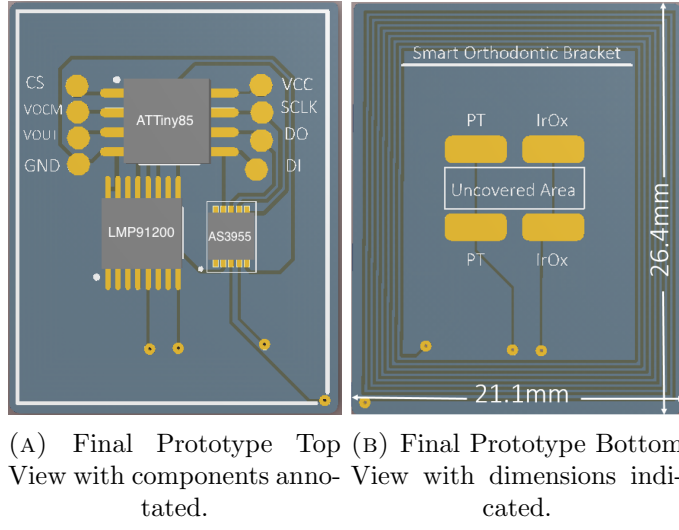


FIGURE 8.2: Final Prototype PCB Design

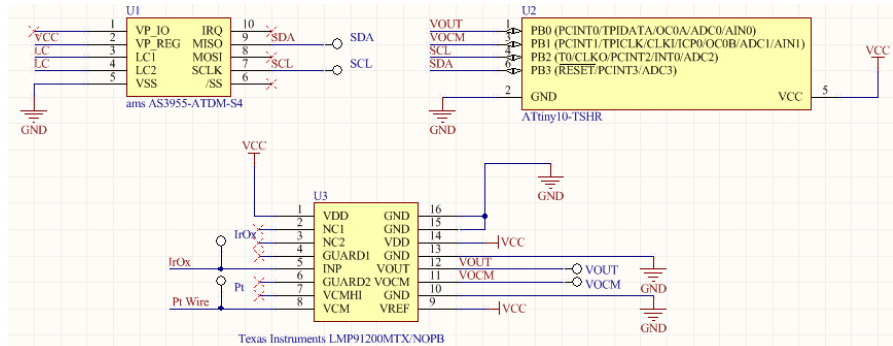


FIGURE 8.3: Final Prototype Schematic

Figure 8.2 shows the top and bottom view of the final prototyped device, while **Figure 8.3** shows the schematic of the final prototype. This is revised slightly from the previous PCB to ensure that the MOSI and MISO pins from the AS3955 pin are correctly connected to the ATTiny85. ADC2 and ADC3 is used instead of ADC2 and ADC0 in order to program the ADCs for differential gain inputs. The antenna used in the device is the optimal antenna tested beforehand at $3.064\mu\text{H}$. The three components(AS3955, ATTiny85 and LMP91200) are then placed in the center on the top side. On the bottom side, the pads are placed for connection with the IrOx and Pt electrodes. The device is fabricated on a FR-4 material, at a 1.55mm thickness for the PCB.



(A) EPO-TEK 301 Kit A(Black) and Kit B(White)

(B) Epoxy Solution

FIGURE 8.4: Encapsulation Solution Set up

8.1.2 Encapsulation of device

In order to place the device in a user's mouth, or in a liquid buffer for testing, the top layer as well as most of the bottom layer has to be covered in a biocompatible material. As shown from the PCB layout, a small area is left uncovered for the electrodes to be exposed to the solution.

The material used for encapsulation of the device is the EPO-TEK 301[63]. This epoxy complies with ISO 10993 biocompatibility testing standards, and is used for encapsulation of FR-4, flex or ceramic PCBs. **Figure 8.4** displays the encapsulation solution.

To create the epoxy, a mixture of the solutions from Kit A and Kit B is mixed in a 1:4 ratio. This is then stirred in a vial as shown in **Figure 8.4**.

The solution is then placed over the prototype, and left to cure in an oven at 65°C. Once this is done, the final device is ready for use.

8.2 Final Prototype Details

A summary of the components used in the final prototype is shown in **Table 8.1**. The number of components used in this device is relatively few. This adds an advantage of being simple to debug in the event of issues, as well as being relatively low priced compared to other commercial options. Most of the components are commercially sourced with the exception of the electrodes.

Due to a PCB manufacturing delay(as of 20/06/17), the device performance would be described during the presentation(26/06/17).

Summary of Components				
No.	Component	Manufacturer	Quantity	Datasheet
1	Iridium Oxide Electrode	CBIT	1	NA
2	Platinum Electrode	CBIT	1	NA
3	ATTiny85	ATMEL	1	[9]
4	AS3955	AMS	1	[6]
5	LMP91200	TI	1	[30]
6	EPO-TEK 301	EPOXY TECHNOLOGY	1	[63]
7	PCB	Eurocircuits	1	
	Dimensions	21.1mm x 26.4 mm		
	Base Material	FR-4		
	Base Material Thickness	1.55mm		
	Base Copper Foil Thickness	12µm/ $\frac{1}{2}$ oz		

TABLE 8.1: Summary of Components

8.3 Chapter Summary and Evaluation

This chapter describes the design of the final prototype, as well as the steps taken in order to encapsulate the device in biocompatible material. Evaluating the final prototype also shows the advantages of the device in comparison to other existing solutions, and its novelty in pH sensing approaches.

The specifications for the final device are shown in **Table 8.2**. As can be seen, the baseline specifications have been met. As this was largely an experimental project with non-detailed specifications, this project has accomplished what it has set out to do.

Finalised Specifications		
No.	Specification	Met?
1	Read pH in the range of 5-8	✓
2	Size of less than 3x3cm for fitting in mouth	✓
3	Transmit Data Wirelessly	✓
4	Obtain Power Wirelessly	✓
5	Biocompatibility	✓

TABLE 8.2: Detailed Specifications for SOB

This project also breaks new ground in terms of small, biocompatible and wireless pH sensors. To date, there has been no previous example of pH sensors with the 3 above-mentioned specifications. Current commercial options for wireless pH sensors only consist of large glass electrodes with inbuilt batteries, and are large and cumbersome for in-vivo usage. On the other hand, of the smaller wireless pH sensors researched from previous papers, the proposed prototype is the smallest. **Table 8.3** compares the proposed prototype with the other proposed sensing methods obtained from prior research.

This work provides a biocompatible wireless pH sensor, capable of monitoring pH values continuously, as well as being able to communicate with any NFC-enabled device. This

Paper	pH Sensing	Continuous?	Power cons.	Size	Frequency	Max Distance	Biocompatible?
[1]	IrOx	Yes	Inductive Coupling	4cm x 3cm	18MHz	18cm	No
[17]	Optical	No	Smartphone Battery	NA	NA	NA	Yes
[18]	Micro pH Electrode	No	Wired Power Supply	NA	NA	NA	Yes
This work	IrOx	Yes	Inductive Coupling	2.1x2.6cm	NFC Standard	32mm	Yes

TABLE 8.3: Comparison with state-of-the-art

has applications in the fields of mobile healthcare, and provides a foundation into future low-powered sensing through NFC devices.

Chapter 9

Conclusion and Future Work

The aim of this project was to design a wireless pH monitoring device that was small enough to be retrofitted in the mouth while being powered through wireless means. To achieve this, research was done on the three key criterias of this project: pH Sensing, energy harvesting and wireless communications.

A variety of pH sensing, energy harvesting and wireless communications methods were compared. The method used was based on specifications of size, biocompatibility and power requirements provided by Dr Christine Mason as well as through previous research. IrOx electrodes were used for the pH sensing component and NFC was used for the power and data transmission. These were determined to be the optimal approach for the device.

Tests were done on each of the modules. The IrOx electrodes in tandem with Pt electrodes showed a linear relation between the voltage output and pH, which made it possible for use as the sensing mechanism. The power requirements of the microcontroller(ATTiny85) used and the read out circuit(LMP91200) required for the IrOx electrodes were deemed to be capable of being met by the AS3955 NFC chip.

In order to fabricate the final prototype, multiple antennas were designed on an experimental PCB to determine if they were able to supply the required power. As the designed antenna was able to meet the power requirements, the final prototype was based on this designed antenna. The experimental PCB was also capable of accurately reading pH values after calibration was done. The PCB for the final prototype was designed, and an encapsulation epoxy is used to ensure the device was biocompatible for placement in a user's mouth.

This project is relatively novel, as the field of wireless pH sensors is currently limited to large glass electrodes. The smallest wireless pH sensor found in papers [1] is larger than

the proposed final prototype, and also requires a proprietary transmitter for the power transfer. In comparison, the proposed device in this paper is smaller, and also able to obtain power from any NFC-enabled Android smartphone. As this project proves the feasibility of applying NFC technology to the field of biomedical technology, a paper will be submitted based on the findings of this paper to BioCAS 2017. Thus, this project would hopefully have applications in the use of NFC for mobile healthcare devices in the future, and serve as a foundation for similar NFC-based sensing devices.

9.1 Future Work

Due to time or equipment limitations, this section would describe the possible future work to be done on this project.

The IrOx and Pt electrodes used decreased in sensitivity from 35mV/pH when they were just fabricated to around 12mV/pH after around 3 months. Although this could be resolved with applying a gain to the ADCs, this would require constant recalibration of the parameters in the microcontroller software. Thus, more work could be done to explore the reason behind this occurrence, and attempt to find a solution to prevent this. It was also found that AgCl electrodes could be fabricated in the form of a thin wire, as done in [1]. The sensitivity of this reference electrode in tandem with an IrOx electrode was around 50mV/pH, and could be looked into as a possible solution.

The current design of the reference voltage relies upon the VDD. As the VDD for the SOB fluctuates depending on the orientation of the tag antenna with the reader antenna, readings may be taken that do not accurately reflect the correct pH value. A possible solution could be to use a capacitor to hold the VDD value constant to prevent fluctuations in the voltage reference. However, more tests need to be done on this to observe the effect on the supply voltage output of the AS3955.

As mentioned previously [Section 4.5](#), the antenna design could be aided with the help of a simulation program. The HFSS software would allow a simulation of a magnetic field, and observe its effects on a designed antenna. In this case, an antenna could be designed to its minimum size where it is still able to supply the power required from a field. This could further improve the sizing of the SOB, and also opens the door for other forms of configuration in the SOB design. The research approach taken in this project involved the use of an iterative experimental approach, with commercial antennas tested before the use of designed PCB antennas were applied. This could change through the use of the software. The antenna used in this experiment was based on the 20x25mm NFC demo tags. As these were the smallest working NFC tags, the antenna was designed

assuming that this was the minimum size possible. However, future work could explore different shaped antenna. Narrow antennas, or antennas that are flexible could be used for this experiment.

A limitation of this experiment would be the use of a single reader from the Nexus 5 smartphone. Hence, most of the readings for power transmitted and obtained from the NFC tags are limited by the power supply of the reader. In addition to this, the NFC characteristics of the transmitter coil of the Nexus 5 is unavailable online, and hence it is difficult to ascertain its repeatability. Future experiments could consider the use of a specified NFC reader, with variable power output. This could allow the variation of the maximum range, as well as the power received by the tag. These was not explored in this experiment, and would be excellent to look into in the future.

The power of the ATTiny85 could be reduced further by actively switching off peripherals that are not used during runtime. In addition to this, the ADC decoding code currently relies on a look up table in order to determine the pH value of the solution. As there is a linear relation between the ADC output and the pH value, a more elegant method would be to use the linear equation in order to approximate the pH values. This could be further explored in future works.

The FR-4 substrate used is a hard substrate, which is unable to flex under pressure. However, there exist other types of PCB substrates that are able to flex, and some that are biocompatible as well. Having flexible substrates allow for experimentation into other forms of placement of the device in the mouth, and biocompatible substrates also reduce the possibility of the device interfering with a user's bodily functions.

Due to the limited timeframe of the project, personnel tests were not conducted. As the SOB may vary in comfort for different mouth sizes, it is important to have an idea about how the device can be modified for different users.

Appendix A

Appendix A: Embedded Software

```
// SOB.c
// ATtiny85 Programming for Smart Orthodontic Bracket
// Input Signals: Vout and Vocm(From LMP91200)
// Output Signals: SPI - MOSI, MISO, CS and SCLK(To AS3955)
/* Libraries -----*/
#include <avr/io.h>          //ATTiny85 Pin Names
#include <avr/interrupt.h>    //Interrupt Library
#include <util/delay.h>        //Delay Utility

/* Pin Definitions -----*/
//SS or CS Pin
#define SS_PIN PB3
#define DD_SS_PIN DDB3
//DI Pin
#define DI_PIN PB0
#define DD_DI_PIN DDB0
//DO Pin
#define DO_PIN PB1
#define DD_DO_PIN DDB1
//SCLK
#define SCLK_PIN PB2
#define DD_SCLK_PIN DDB2

/* Function
Declarations-----*/
void initSPI();
unsigned char SPI_write(unsigned char);
void SPI_test();
void setclock();
```

```
void AS3955_voltage();
int8_t VOUT_VOCM();
void write_NDEF(uint8_t, uint8_t);
uint8_t decode_ADC(int8_t);

/* Main Function-----*/
//Function that runs on microcontroller startup
int main (void)
{
    setclock(); //Lowers frequency to save power
    initSPI(); //Initialise SPI for comms with NFC chip

    int vdiff = VOUT_VOCM();           //Take inputs from ADC
    uint8_t pH = decode_ADC(vdiff);    //Decoding ADC values to approximate
    pH values
    write_NDEF(0x04,pH);             //Write NDEF message to AS3955

    while (1)
    {
    }
    return 1;
}
/* Public Functions-----*/

/* Function: This function initialises the clock speed
 * Parameters: None
 * Inputs: None
 * Outputs: None
 */
void setclock()
{
    CLKPR = 0x80; //To enable clock changes
    CLKPR = 0b00000011;//clock divide by 8 to 1Mhz(125kHz measured on clock
    cycle)
}

/* Function: This function initialises the SPI interface
 * Parameters: None
 * Inputs: None
 * Outputs: None
 */
void initSPI()
{
    //Outputs
    DDRB |= (1<<DD_DO_PIN) | (1 <<DD_SCLK_PIN) | (1 <<DD_SS_PIN);
```

```

//Inputs
DDRB &= ~(1<<DD_DI_PIN);
//SPI Config for USI Interface(0 for I2C)
USICR = (1<<USIWMO);
//SS Pin high, MISO enable pullup
PORTB |= (1<<DI_PIN) | (1 << SS_PIN);
//PORTB |= (1<<SS_PIN) | (1<<DI_PIN);
}

/* Function: This function transmits a byte through the SPI interface and
   returns data received if data is sent
* Parameters: None
* Inputs: uchar data(byte to be transmitted)
* Outputs: uchar USIDR(received data stored in data register)
*/
unsigned char SPI_write(unsigned char data)
{
    //load USI Data Register with data to transmit
    USIDR = data; // data
    USISR = (1<<USIOIF); //Clear Flag(Check again exactly what)
    do {
        USICR = (1<<USIWMO) | (1<<USICS1) | (1<<USICLK) | (1<<USITC);
    } while ((USISR & (1<<USIOIF)) == 0);
    return USIDR;
}

/* Function: This function sets the output voltage of the AS3955 at 3.3V
* Parameters: None
* Inputs: None
* Outputs: None
*/
void AS3955_voltage()
{
    PORTB &= ~(1<<SS_PIN); //bring down CS Pin
    SPI_write(0x40); //mode
    SPI_write(0xFE); //block address
    SPI_write(0x3B); //Message Type, 0x03 for NDEF (T field)
    SPI_write(0x80); //Number of bytes in message (L field)
    SPI_write(0x00); //start message (V field)
    SPI_write(0x00);
    PORTB |= (1<<SS_PIN); //Bring up CS Pin
}

//This function returns the differential output from ADC2 and ADC3
//Outputs: int8_t Vdiff(voltage difference in millivolts)
/* Function: This function sets the output voltage of the AS3955 at 3.3V
* Parameters: None

```

```

* Inputs:    None
* Outputs:   None
*/
int8_t ADC2_ADC3()
{
    //Initialising ADC2 and ADC3 for gain input, ADC2 positive and ADC3
    //negative. 0110 for x1 gain, 0111 for x20gain
    ADMUX =
        (1 << ADLAR) |      // left shift result (for 8-bit values)
        (1 << REFS2) |      // Sets ref. voltage to internal 2.56V, bit 2
        (1 << REFS1) |      // Sets ref. voltage to internal 2.56V, bit 1
        (0 << REFS0) |      // Sets ref. voltage to internal 2.56V, bit 0
        (0 << MUX3) |      // use ADC2/3 for input , MUX bit 3
        (1 << MUX2) |      // use ADC2/3 for input , MUX bit 2
        (1 << MUX1) |      // use ADC2/3 for input , MUX bit 1
        (0 << MUX0);      // use ADC2/3 for input , MUX bit 0

    ADCSRA =
        (1 << ADEN) |      // Enable ADC
        (1 << ADPS2) |      // set prescaler to 16, bit 2
        (0 << ADPS1) |      // set prescaler to 16, bit 1
        (0 << ADPS0);      // set prescaler to 16, bit 0

    ADCSRA |= (1 << ADSC);           // start ADC measurement
    while (ADCSRA & (1 << ADSC) ); // wait till conversion complete
    int Vdiff;
    Vdiff = ADCH * 2560/512; //Gives the value of Vpos-Vneg = ADC2 - ADC3 in
    //millivolts
    return Vdiff;
}

/* Function: Function that returns result of ADC2 - ADC0 readings(Only for
experimental PCB)
* Parameters:  None
* Inputs:      None
* Outputs:    uint8_t Vdiff
*/
uint8_t VOUT_VOCM()
{
    //ADC2 VOUT readings
    ADMUX =
        (1 << ADLAR) |      // left shift result (for 8-bit values)
        (1 << REFS2) |      // Sets ref. voltage to VCC, bit 2
        (1 << REFS1) |      // Sets ref. voltage to VCC, bit 1

```

```

(0 << REFS0) |      // Sets ref. voltage to VCC, bit 0
(0 << MUX3) |      // use ADC2 for input (PB4), MUX bit 3
(0 << MUX2) |      // use ADC2 for input (PB4), MUX bit 2
(1 << MUX1) |      // use ADC2 for input (PB4), MUX bit 1
(0 << MUX0);       // use ADC2 for input (PB4), MUX bit 0

ADCSRA =
(1 << ADEN) |      // Enable ADC
(1 << ADPS2) |      // set prescaler to 16, bit 2
(0 << ADPS1) |      // set prescaler to 16, bit 1
(0 << ADPS0);       // set prescaler to 16, bit 0

ADCSRA |= (1 << ADSC);           // start ADC measurement
while (ADCSRA & (1 << ADSC) ); // wait till conversion complete

// for 10-bit resolution:
int Vout;
Vout = ADCH;

//ADC0 VOCM Readings
ADMUX =
(1 << ADLAR) |      // left shift result (for 8-bit values)
(1 << REFS2) |      // Sets ref. voltage to internal 1.1V, bit 2
(1 << REFS1) |      // Sets ref. voltage to internal 1.1V, bit 1
(0 << REFS0) |      // Sets ref. voltage to internal 1.1V, bit 0
(0 << MUX3) |      // use ADC2 for input (PB4), MUX bit 3
(0 << MUX2) |      // use ADC2 for input (PB4), MUX bit 2
(0 << MUX1) |      // use ADC2 for input (PB4), MUX bit 1
(0 << MUX0);       // use ADC2 for input (PB4), MUX bit 0

ADCSRA =
(1 << ADEN) |      // Enable ADC
(1 << ADPS2) |      // set prescaler to 16, bit 2
(0 << ADPS1) |      // set prescaler to 16, bit 1
(0 << ADPS0);       // set prescaler to 16, bit 0

ADCSRA |= (1 << ADSC);           // start ADC measurement
while (ADCSRA & (1 << ADSC) ); // wait till conversion complete

// for 10-bit resolution:
int Vocm, Vdiff;
Vocm = ADCH;

```

```
Vdiff = Vout-Vocm;
return Vdiff;

}

/* Function: This function approximates the pH value from a straight line
relation using the VOUT-VOCM values.

* Parameters: linearity(mV), offset value at pH5(mV)
* Inputs: int8_t VOUT-VOCM (in millivolts)
* Outputs: uint8_t pH
*/
uint8_t decode_ADC(int8_t VOUT_VOCM)
{
    uint8_t pH;
    int8_t offset = 75; //Set from Ir0x and Pt readings
    int8_t linearity = 33; //Set from Ir0x and Pt readings

    if(VOUT_VOCM > offset)
    {
        pH = 0x00; //More than expected voltage value - check offset
    }
    else if(VOUT_VOCM > (offset - (linearity/10)))
    {
        pH = 0x50; //pH is 5.0
    }
    else if(VOUT_VOCM > (offset - 2*(linearity/10)))
    {
        pH = 0x51; //pH is 5.1
    }
    else if(VOUT_VOCM > (offset - 3*(linearity/10)))
    {
        pH = 0x52; //pH is 5.2
    }
    else if(VOUT_VOCM > (offset - 4*(linearity/10)))
    {
        pH = 0x53; //pH is 5.3
    }
    else if(VOUT_VOCM > (offset - 5*(linearity/10)))
    {
        pH = 0x54; //pH is 5.4
    }
    else if(VOUT_VOCM > (offset - 6*(linearity/10)))
    {
```

```
pH = 0x55; //pH is 5.5
}
else if(VOUT_VOCM > (offset - 7*(linearity/10)))
{
    pH = 0x56; //pH is 5.6
}
else if(VOUT_VOCM > (offset - 8*(linearity/10)))
{
    pH = 0x57; //pH is 5.7
}
else if(VOUT_VOCM > (offset - 9*(linearity/10)))
{
    pH = 0x58; //pH is 5.8
}
else if(VOUT_VOCM > (offset - 10*(linearity/10)))
{
    pH = 0x59; //pH is 5.9
}
else if(VOUT_VOCM > (offset - 11*(linearity/10)))
{
    pH = 0x60; //pH is 6.0
}
else if(VOUT_VOCM > (offset - 12*(linearity/10)))
{
    pH = 0x61; //pH is 6.1
}
else if(VOUT_VOCM > (offset - 13*(linearity/10)))
{
    pH = 0x62; //pH is 6.2
}
else if(VOUT_VOCM > (offset - 14*(linearity/10)))
{
    pH = 0x63; //pH is 6.3
}
else if(VOUT_VOCM > (offset - 15*(linearity/10)))
{
    pH = 0x64; //pH is 6.4
}
else if(VOUT_VOCM > (offset - 16*(linearity/10)))
{
    pH = 0x65; //pH is 6.5
}
else if(VOUT_VOCM > (offset - 17*(linearity/10)))
{
```

```
pH = 0x66; //pH is 6.6
}
else if(VOUT_VOCM > (offset - 18*(linearity/10)))
{
    pH = 0x67; //pH is 6.7
}
else if(VOUT_VOCM > (offset - 19*(linearity/10)))
{
    pH = 0x68; //pH is 6.8
}
else if(VOUT_VOCM > (offset - 20*(linearity/10)))
{
    pH = 0x69; //pH is 6.9
}
else if(VOUT_VOCM > (offset - 21*(linearity/10)))
{
    pH = 0x70; //pH is 7.0
}
else if(VOUT_VOCM > (offset - 22*(linearity/10)))
{
    pH = 0x71; //pH is 7.1
}
else if(VOUT_VOCM > (offset - 23*(linearity/10)))
{
    pH = 0x72; //pH is 7.2
}
else if(VOUT_VOCM > (offset - 24*(linearity/10)))
{
    pH = 0x73; //pH is 7.3
}
else if(VOUT_VOCM > (offset - 25*(linearity/10)))
{
    pH = 0x74; //pH is 7.4
}
else if(VOUT_VOCM > (offset - 26*(linearity/10)))
{
    pH = 0x75; //pH is 7.5
}
else if(VOUT_VOCM > (offset - 27*(linearity/10)))
{
    pH = 0x76; //pH is 7.6
}
else if(VOUT_VOCM > (offset - 28*(linearity/10)))
{
```

```
pH = 0x77; //pH is 7.7
}
else if(VOUT_VOCM > (offset - 29*(linearity/10)))
{
    pH = 0x78; //pH is 7.8
}
else if(VOUT_VOCM > (offset - 30*(linearity/10)))
{
    pH = 0x79; //pH is 7.9
}
else if(VOUT_VOCM > (offset - 31*(linearity/10)))
{
    pH = 0x80; //pH is 8.0
}
else if(VOUT_VOCM > (offset - 32*(linearity/10)))
{
    pH = 0x81; //pH is 8.1
}
else if(VOUT_VOCM > (offset - 33*(linearity/10)))
{
    pH = 0x82; //pH is 8.2
}
else if(VOUT_VOCM > (offset - 34*(linearity/10)))
{
    pH = 0x83; //pH is 8.3
}
else if(VOUT_VOCM > (offset - 35*(linearity/10)))
{
    pH = 0x84; //pH is 8.4
}
else if(VOUT_VOCM > (offset - 36*(linearity/10)))
{
    pH = 0x85; //pH is 8.5
}
else if(VOUT_VOCM > (offset - 37*(linearity/10)))
{
    pH = 0x86; //pH is 8.6
}
else if(VOUT_VOCM > (offset - 38*(linearity/10)))
{
    pH = 0x87; //pH is 8.7
}
else if(VOUT_VOCM > (offset - 39*(linearity/10)))
{
```

```
pH = 0x88; //pH is 8.8
}
else if(VOUT_VOCM > (offset - 40*(linearity/10)))
{
    pH = 0x89; //pH is 8.9
}
else if(VOUT_VOCM > (offset - 41*(linearity/10)))
{
    pH = 0x90; //pH is 9.0
}
else
{
    pH = 0xFF; //less than expected value, indicates error
}
return pH;
}

/* Function: This function writes an NDEF message to the AS3955 EEPROM.
 * Parameters: None
 * Inputs: uint8_t address, uint8_t data
 * Outputs: None
 */
void write_NDEF(uint8_t address, uint8_t data)//Writes an NDEF message to a
    block
{
    PORTB &= ~(1<<SS_PIN); //bring down CS Pin
    SPI_write(0x40); //mode
    SPI_write(address<<1); //block address
    SPI_write(0x03); //Message Type, 0x03 for NDEF (T field)
    SPI_write(0x02); //Number of bytes in message (L field)
    SPI_write(0x00); //start message (V field)
    SPI_write(data);
    PORTB |= (1<<SS_PIN); //Bring up CS Pin
}
```

Bibliography

- [1] Sharmistha Bhadra, Damaris SY Tan, Douglas J Thomson, Michael S Freund, and Greg E Bridges. A wireless passive sensor for temperature compensated remote ph monitoring. *IEEE Sensors Journal*, 13(6):2428–2436, 2013.
- [2] ph meter information, 2017. URL <http://www.ph-meter.info/>.
- [3] Paul D Mitcheson. Energy harvesting for human wearable and implantable bio-sensors. In *Engineering in Medicine and Biology Society (EMBC), 2010 Annual International Conference of the IEEE*, pages 3432–3436. IEEE, 2010.
- [4] Kazuya Goto, Tetsuya Nakagawa, Osamu Nakamura, and Satoshi Kawata. An implantable power supply with an optically rechargeable lithium battery. *IEEE Transactions on Biomedical Engineering*, 48(7):830–833, 2001.
- [5] Jacopo Olivo, Sandro Carrara, and Giovanni De Micheli. Energy harvesting and remote powering for implantable biosensors. *IEEE Sensors Journal*, 11(7):1573–1586, 2011.
- [6] ams AG. next-generation nfc interface tag ic with advanced data and energy management features, 2017. URL <http://ams.com/eng/Products/Wireless-Connectivity/Sensor-Tags-Interfaces/AS3955>.
- [7] An2866 - how to design a 13.56mhz customized tag antenna, 2009. URL <http://www.proxmark.org/files/Documents/Antennas/How%20to%20design%20a%2013.56%20MHz%20customized%20tag%20antenna.pdf>.
- [8] nfc design navi — specific use logic lsi — production — semiconductor — panasonic 2012, 2012. URL <https://b2bsol.panasonic.biz/semi-spt/apl/en/tool/nfcdesignnavigator/>.
- [9] Attiny85 - microcontrollers and processors, 2017. URL <http://www.microchip.com/wwwproducts/en/ATtiny85>.
- [10] Gauri S Desai and Suresh T Mathews. Saliva as a non-invasive diagnostic tool for inflammation and insulin-resistance. *World J Diabetes*, 5(6):730–738, 2014.

- [11] Sharmila Baliga, Sangeeta Muglikar, Rahul Kale, et al. Salivary ph: A diagnostic biomarker. *Journal of Indian Society of Periodontology*, 17(4):461, 2013.
- [12] Christine m. mason dds, 2017. URL
<http://www.stjohnsmidentist.com/christine-m-mason-dds.html>.
- [13] How orthodontic braces work, 2017. URL <http://kygerorthodontics.com/blog/patienteducation/how-orthodontic-braces-work/>.
- [14] How to test your bodys ph (saliva and urine), 2017. URL
<https://www.alkaway.com.au/learning-centre/alkaline-diet-and-health/how-to-test-your-bodys-ph-saliva-urine/>.
- [15] Wireless ph sensor:ps3204, 2017. URL [https://www.pasco.com/prodCatalog/PS/\\$PS-3204_wireless-ph-sensor\\$/index.cfm](https://www.pasco.com/prodCatalog/PS/$PS-3204_wireless-ph-sensor$/index.cfm).
- [16] Vernier. Go wireless ph, 2017. URL
<https://www.vernier.com/products/sensors/ph-sensors/gw-ph/>.
- [17] Vlad Oncescu, Dakota O'Dell, and David Erickson. Smartphone based health accessory for colorimetric detection of biomarkers in sweat and saliva. *Lab on a Chip*, 13(16):3232–3238, 2013.
- [18] JM Davidson, RST Linforth, and AJ Taylor. In-mouth measurement of ph and conductivity during eating. *Journal of agricultural and food chemistry*, 46(12):5210–5214, 1998.
- [19] Sigma-aldrich micro ph combination electrode, glass body, 2017. URL
<http://www.sigmapellic.com/catalog/product/aldrich/z113441?lang=en®ion=GB>.
- [20] Imperial College London. Centre for bio-inspired technology, June 2017. URL
<http://www.imperial.ac.uk/bio-inspired-technology>.
- [21] Sara S Ghoreishizadeh, Pantelis Georgiou, Sandro Carrara, and Giovanni De Micheli. An integrated platform for differential electrochemical and isfet sensing. In *Circuits and Systems (ISCAS), 2016 IEEE International Symposium on*, pages 2875–2878. IEEE, 2016.
- [22] Claudio Zuliani, Fu Siong Ng, Andrea Alenda, Amir Eftekhar, Nicholas S Peters, and Christofer Toumazou. An array of individually addressable micro-needles for mapping ph distributions. *Analyst*, 141(15):4659–4666, 2016.
- [23] Sigma aldrich glass reference electrode, 2017. URL <http://www.sigmapellic.com/catalog/product/aldrich/z113093?lang=en®ion=GB>.

- [24] JEON Dayeong, YOO Wook Jae, SEO Jeong Ki, SHIN Sang Hun, HAN Ki-Tek, KIM Seon Geun, PARK Jang-Yeon, and LEE Bongsoo. Fiber-optic ph sensor based on sol-gel film immobilized with neutral red. *Optical review*, 20(2):209–213, 2013.
- [25] Steven Washington. Optical ph sensors, 2017. URL <http://www.all-about-ph.com/optical-ph-sensors.html>.
- [26] Peter Kurzweil. Metal oxides and ion-exchanging surfaces as ph sensors in liquids: State-of-the-art and outlook. *Sensors*, 9(6):4955–4985, 2009.
- [27] Analog Devices. Op290 datasheet, 2017. URL <http://www.analog.com/en/products/amplifiers/operational-amplifiers/high-voltage-amplifiers-greaterthanequalto-12v/op290.html>.
- [28] Power Electronics. Texas instruments’ (national semiconductor) lm series linear products re-introduced, 2014. URL <http://www.powerelectronics.com/power-management/texas-instruments-national-semiconductor-lm-series-linear-products-re-introduced>.
- [29] Linear Technology. Lt1126 - dual decompensated low noise, high speed precision op amps, 2017. URL <http://www.linear.com/product/LT1126>.
- [30] Texas Instruments. Lmp91200 integrated afe for low-power ph sensing applications, 2017. URL <http://www.ti.com/product/LMP91200>.
- [31] Texas Instruments. Wireless ph sensor transmitter, 2017. URL <http://www.ti.com/lit/ug/tidua47b/tidua47b.pdf>.
- [32] Ming-Zhi Yang, Chyan-Chyi Wu, Ching-Liang Dai, and Wen-Jung Tsai. Energy harvesting thermoelectric generators manufactured using the complementary metal oxide semiconductor process. *Sensors*, 13(2):2359–2367, 2013.
- [33] Michail E Kiziroglou, Steven W Wright, Tzern T Toh, Paul D Mitcheson, Th Becker, and Eric M Yeatman. Design and fabrication of heat storage thermoelectric harvesting devices. *IEEE Transactions on Industrial Electronics*, 61(1):302–309, 2014.
- [34] Evident Thermoelectrics. End use applications, 2017. URL <https://evidentthermo.com/>.
- [35] Paul D Mitcheson, Eric M Yeatman, G Kondala Rao, Andrew S Holmes, and Tim C Green. Energy harvesting from human and machine motion for wireless electronic devices. *Proceedings of the IEEE*, 96(9):1457–1486, 2008.

- [36] Christian Sauer, Milutin Stanacevic, Gert Cauwenberghs, and Nitish Thakor. Power harvesting and telemetry in cmos for implanted devices. *IEEE Transactions on Circuits and Systems I: Regular Papers*, 52(12):2605–2613, 2005.
- [37] Tayfun Akin, Khalil Najafi, and Robert M Bradley. A wireless implantable multichannel digital neural recording system for a micromachined sieve electrode. *IEEE Journal of solid-state circuits*, 33(1):109–118, 1998.
- [38] Kanber Mithat Silay, Catherine Dehollain, and Michel Declercq. A closed-loop remote powering link for wireless cortical implants. *IEEE Sensors Journal*, 13(9):3226–3235, 2013.
- [39] Michael Catrysse, Bart Hermans, and Robert Puers. An inductive power system with integrated bi-directional data-transmission. *Sensors and Actuators A: Physical*, 115(2):221–229, 2004.
- [40] Gregory Melia. *Electromagnetic Absorption by the Human Body from 1-15 GHz*. PhD thesis, University of York, 2013.
- [41] Ada SY Poon, Stephen O’Driscoll, and Teresa H Meng. Optimal frequency for wireless power transmission into dispersive tissue. *IEEE Transactions on Antennas and Propagation*, 58(5):1739–1750, 2010.
- [42] Sami Gabriel, RW Lau, and Camelia Gabriel. The dielectric properties of biological tissues: Iii. parametric models for the dielectric spectrum of tissues. *Physics in medicine and biology*, 41(11):2271, 1996.
- [43] ANSYS. Ansys hfss, 2017. URL
<http://www.ansys.com/products/electronics/ansys-hfss>.
- [44] P1110b 915 mhz rf powerharvester product datasheet, 2017. URL
<http://www.mouser.co.uk/pdfdocs/P1110B-datasheet.pdf>.
- [45] ams AG. Epc sensor tag and data logger ic - ams sl900a, 2017. URL
<http://ams.com/eng/Products/Wireless-Connectivity/Sensor-Tags-Interfaces/SL900A>.
- [46] Rf430frl152h nfc iso15693 sensor transponder with spi/i2c interface and 14-bit sigma-delta adc, 2017. URL <http://www.ti.com/product/RF430FRL152H>.
- [47] Craig Tadlock. Will apple support nfc tags in ios 10 for the iphone 7?, 2017. URL
<https://gototags.com/blog/will-apple-finally-support-nfc-tag-reading-ios-10-iphone-7/>.

- [48] Mamoru Akimoto and Masataka Iizuka. Load modulation applied to magnetic resonance wireless power transfer technology and its applications — ntt technical review, 2017. URL <https://www.ntt-review.jp/archive/ntttechnical.php?contents=ntr201310ra1.html>.
- [49] Klaus Finkenzeller. Rfid-handbook - active load modulation, 2017. URL <http://rfid-handbook.de/about-rfid/active-load-modulation.html?showall=1>.
- [50] Hf antenna design notes, 2003. URL <http://www.ti.com/lit/an/scba034/scba034.pdf>.
- [51] ABRACON CORPORATION. Abracon ptm - introduction to anfca series - flexible peel and stick nfc antennas, 2017. URL <http://www.abracon.com/Support/ANFCA-PTM.pdf>.
- [52] Pulse Corporation and LB Q39G-L2OO-35-1. W7001 pulse electronics corporation — rf/if and rfid — digikey, 2017. URL <https://www.digikey.com/product-detail/en/pulse-electronics-corporation/W7001/553-2633-ND/4169647>.
- [53] Abracon LLC. Anfca-3225-a02 abracon llc — rf/if and rfid — digikey, 2017. URL <https://www.digikey.com/product-detail/en/abracon-llc/ANFCA-3225-A02/535-12515-ND/4864624>.
- [54] Abracon LLC. Anfca-1510-a02 abracon llc — rf/if and rfid — digikey, 2017. URL <https://www.digikey.co.uk/product-detail/en/abracon-llc/ANFCA-1510-A02/535-12517-ND/4864626>.
- [55] Abracon LLC. Anfca-2515-a02 abracon llc — rf/if and rfid — digikey, 2017. URL <https://www.digikey.com/product-detail/en/abracon-llc/ANFCA-2515-A02/535-12516-ND/4864625>.
- [56] Abracon LLC. Anfca-2525-a02 abracon llc — rf/if and rfid — digikey, 2017. URL <https://www.digikey.co.uk/product-detail/en/abracon-llc/ANFCA-2525-A02/ANFCA-2525-A02-ND/4864656>.
- [57] Attiny10 - microcontrollers and processors, 2017. URL <http://www.microchip.com/wwwproducts/en/ATtiny10>.
- [58] Attiny20 - microcontrollers and processors, 2017. URL <http://www.microchip.com/wwwproducts/en/ATtiny20>.
- [59] Attiny102 - microcontrollers and processors, 2017. URL <http://www.microchip.com/wwwproducts/en/ATtiny102>.

- [60] phydron buffer chemvelopes, 2017. URL <https://www.microessentiallab.com>.
- [61] Steven Washington. How a ph meter works, 2017. URL <http://www.all-about-ph.com/optical-ph-sensors.html>.
- [62] Pasi Raumonen, Lauri Sydanheimo, Leena Ukkonen, M Keskilammi, and M Kivikoski. Folded dipole antenna near metal plate. In *Antennas and Propagation Society International Symposium, 2003. IEEE*, volume 1, pages 848–851. IEEE, 2003.
- [63] Epo-tek 301, 2017. URL [http://www.epotek.com/site/component/products/productdetail.html?cid\[0\]=231](http://www.epotek.com/site/component/products/productdetail.html?cid[0]=231).